



LAWRENCE  
LIVERMORE  
NATIONAL  
LABORATORY

# Removing Orbital Debris With Lasers

C. R. Phipps, K. L. Baker, S. B. Libby, D. A. Liedahl, S.  
S. Olivier, L. D. Pleasance, A. Rubenchik, J. E. Trebes,  
E. V. George, B. Marcovici, J. P. Reilly, M. T. Valley

August 15, 2011

Advances in Space Research

## **Disclaimer**

---

This document was prepared as an account of work sponsored by an agency of the United States government. Neither the United States government nor Lawrence Livermore National Security, LLC, nor any of their employees makes any warranty, expressed or implied, or assumes any legal liability or responsibility for the accuracy, completeness, or usefulness of any information, apparatus, product, or process disclosed, or represents that its use would not infringe privately owned rights. Reference herein to any specific commercial product, process, or service by trade name, trademark, manufacturer, or otherwise does not necessarily constitute or imply its endorsement, recommendation, or favoring by the United States government or Lawrence Livermore National Security, LLC. The views and opinions of authors expressed herein do not necessarily state or reflect those of the United States government or Lawrence Livermore National Security, LLC, and shall not be used for advertising or product endorsement purposes.

## Removing Orbital Debris With Lasers

Claude R. Phipps<sup>‡a</sup>, Kevin L. Baker<sup>b</sup>, Stephen B. Libby<sup>b</sup>, Duane A. Liedahl<sup>b</sup>, Scot S. Olivier<sup>b</sup>, Lyn D. Pleasance<sup>b</sup>, Alexander Rubenchik<sup>b</sup>, James E. Trebes<sup>b</sup>, E. Victor George<sup>c</sup>, Bogdan Marcovici<sup>d</sup>, James P. Reilly<sup>e</sup> and Michael T. Valley<sup>f</sup>

<sup>a</sup> Photonic Associates, LLC, Santa Fe, NM, USA 87508,

[[crhipps@photonicassociates.com](mailto:crhipps@photonicassociates.com)] phone and fax: +1505-466-3877

<sup>b</sup> Lawrence Livermore National Laboratory, Livermore CA 94550 [ [baker7@llnl.gov](mailto:baker7@llnl.gov), [libby1@llnl.gov](mailto:libby1@llnl.gov), [liedahl1@llnl.gov](mailto:liedahl1@llnl.gov), [olivier1@llnl.gov](mailto:olivier1@llnl.gov), [pleasanceld@aol.com](mailto:pleasanceld@aol.com), [rubenchik1@llnl.gov](mailto:rubenchik1@llnl.gov), [trebes1@llnl.gov](mailto:trebes1@llnl.gov) ]

<sup>c</sup> Centech, Carlsbad CA 92011 [ [evictorgeorge@yahoo.com](mailto:evictorgeorge@yahoo.com) ]

<sup>d</sup> System Engineering Associates, El Segundo CA [ [bmarcovici@msn.com](mailto:bmarcovici@msn.com) ]

<sup>e</sup> Northeast Science and Technology, Williamsburg, VA 23188 [ [jpr138@aol.com](mailto:jpr138@aol.com) ]

<sup>f</sup> Sensing and Imaging Technologies Department, Sandia National Laboratories, Albuquerque NM 87123 [ [mtvalle@sandia.gov](mailto:mtvalle@sandia.gov) ]

**Abstract:** Orbital debris in low Earth orbit (LEO) are now sufficiently dense that the use of LEO space is threatened by runaway collision cascading. A problem predicted more than thirty years ago, the threat from debris larger than about 1cm demands serious attention. A promising proposed solution uses a high power pulsed laser system on the Earth to make plasma jets on the objects, slowing them slightly, and causing them to re-enter and burn up in the atmosphere. In this paper, we reassess this approach in light of recent advances in low-cost, light-weight modular design for large mirrors, calculations of laser-induced orbit changes and in design of repetitive, multi-kilojoules lasers, that build on inertial fusion research. These advances now suggest that laser orbital debris removal (LODR) is the most cost-effective way to mitigate the debris problem. No other solutions have been proposed that address the whole problem of large and small debris. A LODR system will have multiple uses beyond debris removal. International cooperation will be essential for building and operating such a system.

**Key Words:** Space debris; laser ablation; orbital debris removal; adaptive optics; segmented mirror design; phase conjugation

### 1.0 Why Debris Clearing is Important

Thirty-five years of poor housekeeping in space have created several hundred thousand pieces of space debris larger than 1cm in the 400 -2000-km altitude low Earth orbit (LEO) band, their density reaching a peak in the 800-1,000-km altitude range (Klinkrad 2006). Debris in the 1- 10-cm size range are most hazardous to LEO space vehicles because they are not tracked, but can cause fatal damage. For objects below 1 cm, "Whipple shields", though expensive, would be effective against hypervelocity impact (Hayhurst et al. 2001), and can be built. The range of debris orbit inclinations gives a most probable closing velocity between

‡ **Corresponding author**

objects (Phipps et al. 1996a) of about 12km/s, a speed at which a piece of debris has ten times the energy density of dynamite. A 100-gram bolt would certainly cause a lethal event on the International Space Station, if it struck the crew chamber. Larger objects present a lesser threat, because they are less numerous (less than 10,000), and can be tracked and usually avoided by maneuvering. Even so, in March, 2009 and again in June, 2011, it was necessary for Space Station astronauts to take cover in a Soyuz capsule to reduce the chance of penetration by an object with unacceptable track uncertainty. Fortunately, the capsule was docked with the Station. Earlier, in February, 2009, an American Iridium satellite collided with a Russian Kosmos satellite, and the resulting cloud of debris combined with that from the Chinese Fengyun 1C ASAT test in January, 2007, to greatly increase the density of debris around the Earth, prompting concerns about the safety of the final Hubble servicing mission. The instability predicted by Kessler and Cour-Palais (Kessler and Cour-Palais 1978) has now reached the point where collisions are on track to become the most dominant debris-generating mechanism. While improved debris tracking and orbit prediction can temporarily improve threat avoidance via maneuvering (Henderson et al. 2011; Sims et al 2011), effective debris clearing strategies will be necessary. Operational models of the changing risks of space debris damage have been developed to analyze costing strategies for debris removal (Bradley and Wein 2009).

## 2.0 Debris Threat Categories and Clearance Strategies

There are about  $N_1 = 2,200$  large objects (diameter  $\geq 100\text{cm}$ , mass of order 1 ton) in LEO, and  $N_2 = 190\text{k}$  small objects (diameter  $\geq 1\text{cm}$ ) (Klinkrad, *ibid.* p. 96). The flux for the small ones in the peak density region (Klinkrad, *ibid.* p 126) is about  $R_2 = 1.4\text{E-}4 \text{ m}^2\text{year}^{-1}$ . Based on the relative numbers, we deduce a flux  $R_1 = 1.7\text{E-}6 \text{ m}^2\text{year}^{-1}$  for the large ones in the LEO band. Taking  $\sigma = 2\text{m}^2$  as the large object cross-section, the interval between collisions of type  $i$  on the large ones across the ensemble is

$$T_{i1} = [\sigma N_i R_i]^{-1} \quad (1)$$

Applying Eq. (1), the chance that a big object will impact a big object is once in  $T_{11} = 134$  years, whereas the chance a small object will impact a big object is once in  $T_{21} = 3$  years. Just removing the big derelicts does not solve the problem. Any new large space asset that is installed in LEO will encounter the same collision rate  $R_{21}$  as before, from the small objects that have not been removed. The lifetime for these small objects at 1000 km altitude is of order 100 years (Phipps et al. 1996b). A system that can address the small objects as well as the big ones is needed.

Both classes need to be addressed because, while the debris growth rate is reduced by removing large derelict objects that produce clouds of debris when hit (Talent 2009), the small-debris threat to a LEO asset is far larger numerically. For example, the chance of a fatal debris-caused Space Station event per decade is about 7% (Teal 1996). Previously, removal of the small debris was underemphasized.

## 3.0 Proposed Solutions to the Debris Problem

Aside from the laser-based approaches, including the pulsed laser ablation method that is the subject of this article, a variety of solutions have been proposed. To name a few, these have included chasing and grappling the object (Bender 2009),

attaching deorbiting kits, deploying nets to capture objects (Hoyt, 2009; Starke et al. 2009) attaching an electrodynamic tether (Kawamoto et al. 2009; Pearson, et al. 2009; Lee, 2009) and deploying clouds of frozen mist (Leavitt 2009), gas (McKnight 2009) or blocks of aerogel (Hamada et al. 2009) in the debris path to slow the debris. While few of these concepts have progressed to the point where costs can be accurately estimated, Bonnal has estimated a cost of 27M\$ per large object (Bonnal 2009) for attaching deorbiting kits. Any mechanical solution will involve a comparable  $\Delta v$ , so we take Bonnal's estimate as representative of the removal cost per large item using mechanical methods.

The mist or unconfined gas solution would have effects that are not debris-specific. A mist or dust cloud deployed in LEO would rapidly disperse, as would a gas detonation, and, if sufficient mass were installed, it would cause existing space platforms as well as derelicts to re-enter.

The gas solution can avoid dispersal, but that requires the deployment of four hundred 100-km diameter balloons in orbit (McKnight 2009). Even if they could be placed so as not to deny space to other assets, they are one-time solutions (one balloon per target) and costly to launch. If made of 5 $\mu$ m Mylar, each 100km balloon would weigh 160 kilotons and cost \$1,600 B to put in orbit using today's launch costs (Phipps et al. 2000).

The aerogel solution has similar problems. It is easy to show that (Phipps 2010) an aerogel "catcher's mitt" solution designed to clear the debris in two years would require a slab 50cm thick and 13 km on a side. Such a slab would have 80-kiloton mass, and would cost \$800M to launch. Even if we ignore the difficulty of maintaining this shape, a fatal problem is the steady 12kN average thrust required to oppose orbital decay of the slab facing ram pressure over an elliptical orbit ranging between 400km and 1100km altitude. To maintain this thrust over a two-year lifetime would require a fuel mass of 150 kilotons, in addition to the mitt mass, tripling the cost.

Laser-based methods can be divided into three general categories distinguished by their goals and laser beam parameters. At the lowest intensities, below the threshold for ablating the debris surface, lasers have been proposed to divert debris through the weak agency of photon momentum (Mason et al. 2011). This approach has laser momentum transfer efficiency four to five orders of magnitude less than pulsed laser ablation. It is problematic because its effects are comparable to the uncertain effects of space weather and sunlight, and does not effectively address the debris growth problem. At higher laser intensity, we can consider heating to ablation with continuous (CW) lasers, but slow heating of tumbling debris will usually give an ablation jet whose momentum contribution cancels itself out, on the average. CW heating causes messy melt ejection rather than clean jet formation, adding to the debris problem. Also, CW lasers cannot reach the required intensity on target at large range without a very small illumination spot size, requiring an unacceptably large mirror.

Pulsed laser orbital debris removal (LODR) was proposed fifteen years ago (Phipps et al. 1996a). The basic setup is illustrated in Figure 1. At that time, lasers as well as telescopes with the required performance did not yet exist, but the

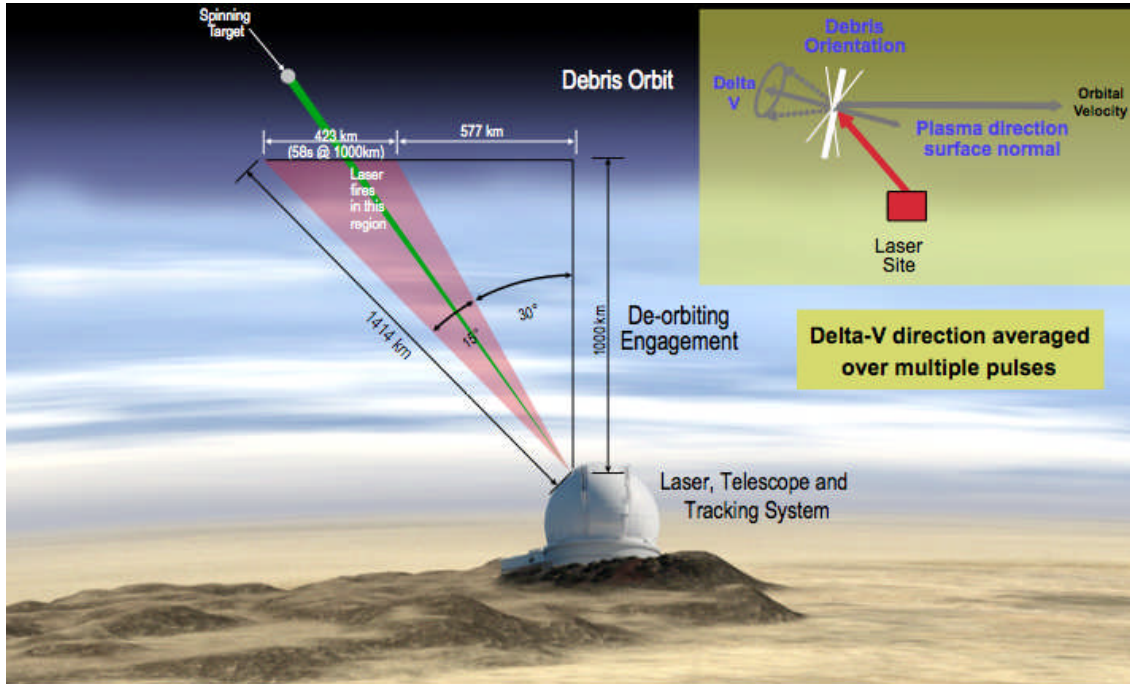


**Figure 1. LODR concept.** The debris target is detected and tracked. Then, a repetitively pulsed laser is focused by a large mirror on it, making a plasma jet. With high intensity, 10 ns pulses, very little target material is removed and the debris is not melted or fragmented. Most of the laser energy goes into the jet. The engagement is designed so the jet points in the right direction to slow the target, on average, by the small amount (100-150 m/s) needed to drop its perigee to 200km, which is adequate for rapid re-entry. Hundreds of pulses are needed to do this, but they can be applied during one pass overhead for the small debris.

components could be specified. Now, all the components actually exist or are in the planning stage.

As recently as four years ago (Liou and Johnson 2006), it was considered that “The use of ground based lasers to perturb the orbits of the satellites is not now practical because of the considerable mass of the satellites and the consequent need to deposit extremely high amounts of energy on the vehicles to effect the necessary change.”

However, we believe that a better understanding of the problem, coupled with advances in technology driven by inertial fusion research, make this statement outdated. The purpose of this article is to demonstrate that laser orbital debris removal is practical and economical.

#### 4.0 How Lasers can Transfer Momentum

The standard measure of the efficiency with which laser light is converted to pressure is the momentum coupling coefficient,

$$C_m = p/I \text{ [Pa W}^{-1}\text{m}^{-2} \text{ or N/W]}. \quad (2)$$

In the ablation regime,  $C_m$  is a function of the laser intensity  $I$ , wavelength  $\lambda$  and laser

pulse duration  $\tau$  and material properties. As the intensity increases,  $C_m$  rises to maximum and decreases at higher laser intensity, because more energy goes into reradiation, ionization, breaking chemical bonds, etc. Figure 2 shows (Sinko and Phipps 2009) this classical behavior. The maximum momentum coupling occurs just at the vapor-plasma transition. In order to design a LODR system, it is crucial to predict the fluency (laser energy per  $m^2$ ) where this maximum is found, and this requires knowing how to combine (Phipps 2011) vapor and plasma models for a particular material. An approximate working relationship is given by (Phipps 2011; Phipps et al. 1988; Phipps et al 2010)

$$\Phi_{opt} = 4.8E8 \sqrt{\tau} \text{ J/m}^2 \quad (3)$$

For  $\tau = 5\text{ns}$ , precise calculations show  $\Phi_{opt} = 53 \text{ kJ/m}^2$  required for an aluminum target (Phipps et al 2010), a worst case.

Multi-kJ laser pulse energy and large mirrors are required to overcome diffraction spreading of the light at a range of 1000km. The spot size  $d_s$  which can be delivered to a target at distance  $z$  is

$$d_s = aM^2\lambda z/D_{eff}. \quad (4)$$

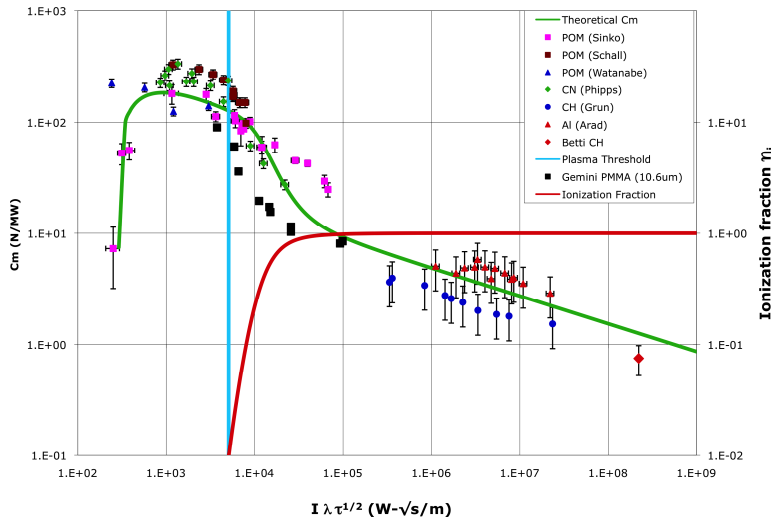


**Figure 2. Example results** of models that allow us to predict  $C_m$  for a number of likely plastics and metals. The vertical blue line shows where the vapor-plasma transition implied by Eq. (2) occurs for  $\text{CO}_2$  lasers, but the  $C_m$  model is universal and applicable to a wide range of laser parameters. The red line is ionization fraction. References for the data are found in Phipps 2010. Reprinted with permission from J. E. Sinko and C. R. Phipps, *Applied Physics Letters*, Vol. 95, page 131105-2j (2009). Copyright 2009, American Institute of Physics.

In Eq. (4),  $M^2$  is the beam quality factor ( $\geq 1$ ),  $D_{eff}$  is the illuminated beam diameter inside the aperture  $D$  for calculating diffraction and  $a$  is a coefficient equal to  $4/\pi$  for a Gaussian beam, or 2.44 for an Airy distribution. A hypergaussian (Phipps et al 1980) with index 6 coming from a LODR system with corrected beam quality  $M^2=2.0$  (Strehl ratio = 0.25) gives  $D_{eff}/D = 0.9$  and  $a = 1.7$ . In order to obtain even  $d_s = 31 \text{ cm}$  at  $z = 1000\text{km}$  range with  $\lambda=1.06\mu\text{m}$  we need  $D_{eff} = 13\text{m}$  illuminated aperture diameter and, to avoid nonlinear

effects in the atmosphere, a minimum  $D_{eff} = 11\text{m}$ . The quantity  $M^2$  in Eq. (4) includes atmospheric phase distortions corrections, either by standard adaptive optics or phase conjugation or a combination of the two (discussed below).

Lightweight mirrors of this size (Egerman et al 2010; Strafford et al 2006) now have a major impact on LODR system design. Examples are the 10-m Keck primary, the 9.8 x 11.1-m South African Large Telescope, and the planned European Extremely Large Telescope with a 42-m diameter primary mirror composed of 984 segments with very low areal mass density (Strafford et al 2006; Strafford 2006).

Denoting the product of all transmission losses, including apodization, physical obscuration by the secondary mirror, spider, coudé path and atmospheric transmission loss by  $T_{\text{eff}}$ , and laser pulse energy by  $W$ , Eq. (4) shows that the product  $WD_{\text{eff}}^2$  required to deliver fluence  $\Phi$  to the target is given by

$$WD_{\text{eff}}^2 = \frac{\pi M^4 a^2 \lambda^2 z^2 \Phi}{4T_{\text{eff}}} \quad (5)$$

In a practical case where  $D_{\text{eff}} = 10\text{m}$ , if  $T = 80\%$ ,  $T_{\text{iff}} = 0.5$ . In order to deliver  $53 \text{ kJ/m}^2$  to a target at  $1000\text{km}$  range, the product  $WD_{\text{eff}}^2$  must be at least  $993 \text{ kJm}^2$ , laser pulse energy must be  $7.3\text{kJ}$ , and the mirror diameter  $D$  must be  $13\text{m}$ .

Predicting the velocity increment  $\Delta\bar{v}$  delivered to a debris object is not a simple matter. It depends on target shape and the orientation of each surface element. The thrust from the plasma jet formed on the target is perpendicular to each element, independent of the angle at which the laser strikes the target. Further, the engagement has to be properly designed to make sure  $\Delta\bar{v}$  is slowing the target rather than speeding it up.

For large targets which can be imaged, we can synchronize the laser pulse with orientation of a target surface element to give an appropriate vector impulse. For small targets, we have no choice but to depend on the averaged impulse from thousands of shots as the target tumbles to give a helpful result. This is aided by the fact that  $C_m$  is dramatically reduced for surface elements at steep angles to the laser beam, as surface-normal intensity drops below optimum [Figure 2]. To simplify discussion, we use an efficiency factor  $\eta_c$  for the combined effects of improper thrust direction, target shape, target tumbling, etc. in reducing the efficiency of laser pulse fluence  $\Phi$  in producing the desired velocity change,

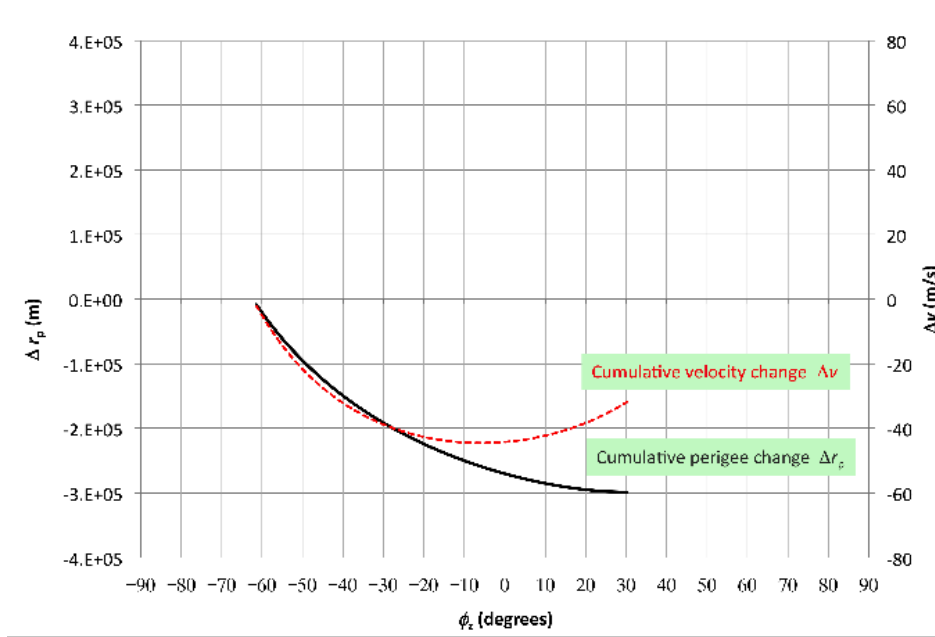
$$\Delta v_{\parallel} = \eta_c C_m \Phi / \mu. \quad (6)$$

In Eq. (6),  $\mu$  is the target areal mass density ( $\text{kg/m}^2$ ). We take  $\eta_c = 0.3$  after Liedahl (Liedahl et al 2010) [see the Appendix for a complete discussion of target shape effects]. The Eq. (6) formulation takes account of laser beam ‘‘overspill’’ for small debris, without having to specify the actual size and mass of each target. In many cases, we can lower the debris perigee not only by pushing antiparallel to its velocity vector, but, counterintuitively, by pushing radially outwards.

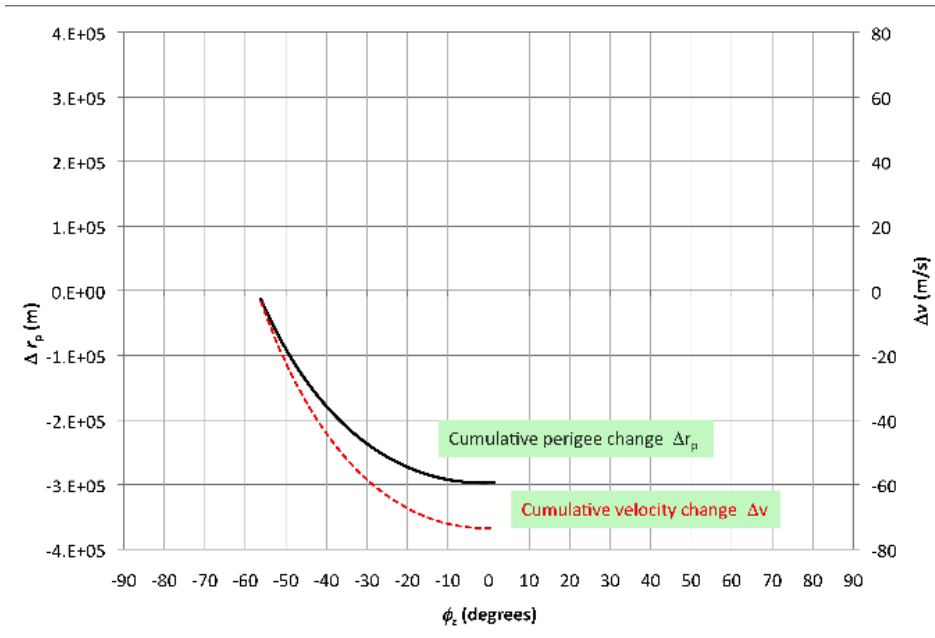
We take  $|\Delta v_o| = 150\text{m/s}$  needed for LEO re-entry and  $\mu = 10\text{kg/m}^2$  for a small target. This value of  $\mu$  is an upper bound average value for small debris (Klinkrad, ibid. p. 70).  $C_m$  can range from  $50$  to  $320 \mu\text{N-s/J}$  just for various surface conditions of aluminum (Esmiller 2011). We have shown  $C_m$  values up to  $300 \mu\text{N-s/J}$  for various organics representative of space debris (Sinko and Phipps 2009). For illustration we use  $C_m = 75 \mu\text{N-s/J}$ . With these values, Eq. (6) shows we have  $\Delta v_{\parallel} = 12\text{cm/s}$  for each

<b>Table 1. Small-target LODR System Parameters</b>			
<b>Target Parameters</b>		<b>Optical System Parameters</b>	
Maximum mass (kg)	0.75	Wavelength $\lambda$ ( $\mu\text{m}$ )	1.06
Areal Mass Density $\mu$ ( $\text{kg}/\text{m}^2$ )	10	Pulse Length $\tau$ (ns)	5
Maximum Range (km)	1,000	$C_m$ ( $\mu\text{N}\cdot\text{s}/\text{J}$ )	75
Perigee Altitude (km)	500	Active mirror diameter $D_b$ (m)	13
Apogee Altitude (km)	700	Spot Size on Target (m)	0.31
Useful Apparition (s)	200	Fluence on Target ( $\text{kJ}/\text{m}^2$ )	75
Minimum Permitted Elevation ( $^\circ$ )	30	Pulse Energy (kJ)	7.3
Retargeting Time (min)	1.0	Repetition Frequency (Hz)	11.2
System Availability (%)	50	Average Optical Power (kW)	81
Number of Targets Accessible	100k	Push Efficiency $\eta_c$	0.30
Time to Re-enter all Targets (mo)	8.7	Average Interaction Duration (s)	100
		Beam Quality Factor	2.0
		Beam Hypergaussian Index	6

<b>Table 2. Large-target LODR System Parameters</b>			
<b>Target Parameters</b>		<b>Optical System Parameters</b>	
Mass (kg)	1,000	Wavelength $\lambda$ ( $\mu\text{m}$ )	1.06
Areal Mass Density $\mu$ ( $\text{kg}/\text{m}^2$ )	820	Pulse Length $\tau$ (ns)	10
Maximum Range (km)	1,500	$C_m$ ( $\mu\text{N}\cdot\text{s}/\text{J}$ )	75
Perigee Altitude (km)	500	Mirror diameter $D_b$ (m)	25
Apogee Altitude (km)	900	Target Spot Size [defocused] (m)	1.25
Useful Apparition (s)	250	Fluence on Target ( $\text{kJ}/\text{m}^2$ )	75
Apparition Interval (days)	10	Pulse Energy (kJ)	140
Minimum Permitted Elevation ( $^\circ$ )	60	Repetition Frequency (Hz)	2.7
Retargeting Time (min)	1.0	Average Optical Power (kW)	370
System Availability (%)	50	Push Efficiency $\eta_c$	0.30
Number of Interactions for Re-entry	135	Average Interaction Duration (s)	250
Time to Re-enter one Target (yrs)	3.7	Beam Quality Factor	2.0
Targets Addressed Per Day	167	Beam Hypergaussian Index	6
Number of Targets	2,200		
Time to Re-enter all Targets (yrs)	4.9		
Effective Re-entry Rate per year	450		



3a.



3b.

**Figure 3. Target re-entry** is achieved in one overhead pass for any debris target smaller than the laser spot radius of 31cm at 1000 km range, having areal mass density  $10\text{kg/m}^2$  or less. The largest target re-entered has 0.75kg mass. Parameters: Wavelength  $1.06 \mu\text{m}$ , beam quality factor 2.0, beam format hypergaussian with index 6, fluence on target  $53 \text{kJ/m}^2$ , 7.3kJ pulse energy, repetition rate 11.2 Hz, mirror diameter 13 m,  $C_m = 75 \mu\text{N-s/J}$ , efficiency factor  $\eta_c = 30\%$ , perigee altitude 500km, apogee altitude 1073km, eccentricity 0.04, re-entry for  $\Delta r_p = -3\text{E}5\text{m}$ . Case a): orbit perigee is -120 degrees geocentric (upstream) relative to laser site, 833 pulses applied all along the debris path over 210 s to achieve minimum perigee. Case b): apogee is overhead the laser site, 1,010 pulses applied over 133 s

laser shot. Taking target availability to be  $T=100s$ , repetition frequency for the 7.3 kJ laser pulse must be  $(\Delta v_o/\Delta v_{||})/T = 12.5Hz$ , for a time-average laser power of 91kW. If the target were as big as the beam focus, it would have 0.75kg mass. Smaller targets of whatever mass with this mass density would also be caused to re-enter in a single overhead pass, even though the beam spills around them.

#### 4.1 Re-entry of Small Targets

Figures (3a) and (3b) show calculations for targets up to 1 kg mass and range up to 1000km being de-orbited in a single overhead pass. Apsidal rotation occurs, but is irrelevant for single-pass re-entry, since the target does not have to be re-acquired. With apogee overhead, only 100 seconds illumination are needed for re-entry. We averaged over the possible orbital orientations to obtain the Table 1 results. The Table 1 system may be considered a “starter system.”

#### 4.2 Re-entry of Large Targets

It has been claimed that lasers cannot de-orbit large, 1-ton derelict debris objects that are of concern. Indeed, single-pass re-entry of these objects is not possible. However, large debris are catalogued and have reasonably accurate ephemerii. Let's consider a 1-ton target with area  $A = 1.25m^2$  presented to the laser (Table 2). With the parameters listed in the Table, it takes 3.7 years to re-enter one object. However, 167 different objects can be addressed in one day, giving 4.9 years to re-enter the whole constellation. Note that it is only necessary (Klinkrad 2009) to re-enter 15 of these large objects annually to *stabilize* the debris environment. From this standpoint alone, the LODR system is a good investment. A larger mirror is required for the large-target system to avoid nonlinear effects in the atmosphere.

### 5.0 Multiple Uses

LODR systems would be useful for purposes other than complete re-entry of all large debris, such as:

#### Increasing ephemeris precision:

Building a LODR system necessitates detection and tracking technology that permits location of targets with 1m precision, far better than present practice. This capability will allow more accurate collision prediction.

#### Orbit modification on demand for large objects:

Even the small-target LODR system would then be able to nudge these objects to avoid collisions, or to provide modest orbit changes, inducing as much as a 35 cm/s velocity change in a 1,000 kg target during a single overhead pass. This is more than required to divert a large target and avoid a predicted collision.

#### Causing precise re-entry:

Re-entry for selected large derelicts can be altered in a calibrated fashion so the re-entry trajectory will endanger neither resident space objects by creating a new potential conjunction, nor air traffic corridors and population locations.

### Moving GEO targets into disposal orbits:

The small target system, coupled with a 10-20m relay mirror just above geosynchronous (GEO) orbit is capable of raising the orbit of a defunct GEO satellite 100km in just 20 minutes.

### **6.0 Acquisition**

An acquisition system reduces the position uncertainty of a debris object from km to the meters required by the “pusher laser” system. A broad field of view staring acquisition telescope with tens of cm aperture using solar target illumination is a valuable adjunct for the LODR system. The best sensor may be a photon counting detector or a charge coupled device (CCD) depending on target luminance (Priedhorsky and Bloch 2005). However, this part of the system is obviously limited to about two hours operation per day.

Active acquisition is possible, in total darkness or in daylight (Phipps et al. 1996b), using the “pusher laser” to illuminate the target, and the LODR system mirror on Earth to collect the scattered light. The accuracy of the U.S. Space Surveillance System would be considered in choosing the field of view for objects that it tracks. For example, with a field of view 3km in diameter at 1000km range, one object per 4 minutes will pass through the field of view, on average. This is enough input for the system. A large (20m) receiving aperture and 7.3kJ pulses from the pusher laser are required to gather enough scattered photons to see small targets. InGaAs focal plane arrays now have quantum efficiencies of 80% (Hansen et al. 2008). In our active tracking system, a 1.5-cm Lambertian scattering target with 50% albedo at 750 km range would return 45 photons to its array pixel on the ground, with a signal to day sky background ratio of 72, on the particular detector pixel to which the 45 laser photons return. The system would require a bandwidth of 0.2nm for both the laser and narrowband optical filter, and a 75 km “range gate.”

The 20-m mirror could have two parts with different optical quality. The central 13m section used by the laser in pusher mode is high quality. The 3.5-m annulus outside that is used to collect light for initial wide field of view acquisition and can be lower quality, since we need only a few-m image precision in the target plane in this mode. If we have a 1000x1000 element array with a 3-km field of view, each pixel projects onto a 3-m spot. Both parts use independently steerable segments about 1m in size mounted on three-point mounts. The outer annulus can be pointed at a different spot from the central portion. Since the target will be moving at about 1 degree/second and within the field of view for only a half-second, each segment is accelerated rapidly over a small angular range while the whole structure comes up to speed. Four independent adaptive optics systems are required [see “Phase Correction” following and Appendix Figure A4].

The optical filter is easy to obtain. Range gating amounts to reading out the array every 250μs and storing the data in slices, delayed from laser firing by the propagation time. This gives rough range information.

### *6.1 Target Tracking*

When the acquisition system has established a track within a 3-km circle, the field of view is narrowed. Ultimately, the computer makes the best focus possible and the pusher laser begins doing its work. The fine tracking signal now becomes very bright and shifts into the blue as plasma is formed on the target. The system uses this signal to stop increasing laser pulse energy. As the field of view is narrowed, the focal plane array is protected from damage with attenuators. Now, the computer makes the best foci possible and the pusher laser begins doing its real work.

### *6.2 Phase Correction via Adaptive Optics*

Phase aberrations are caused by several mechanisms, from thermal distortions in the laser amplifier to atmospheric turbulence. The conventional solution is adaptive optics (Beckers 1993), in which a deformable phase plate with many computer-driven actuators compensates for these distortions as they occur, at a rate of about 1kHz (Appendix). The phase reference for such a system is provided by a “guidestar.” Examples are a 100W beam at 589nm that creates a starlike reference point source in the Earth’s sodium layer at 90km altitude, and the reflection from the target itself.

### *6.3 Look-ahead*

The finite velocity of light requires dealing with “look-ahead” before an accurately tracked target can be “pushed.” At 7.5km/s, the debris is actually as much as 50 m ahead of where the sensor last detected it. Range information is needed to tell the computer how much to correct pointing for the pusher shot, because the target’s actual speed and distance are critical variables. The tracking system outlined above can do this.

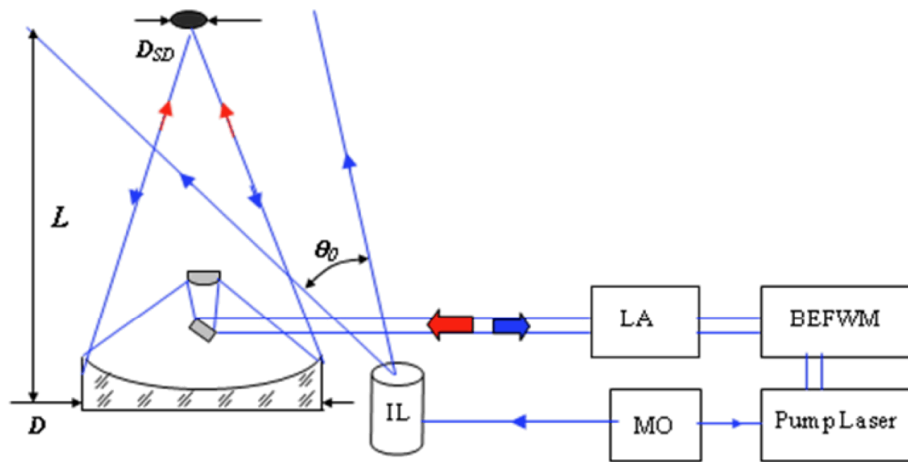
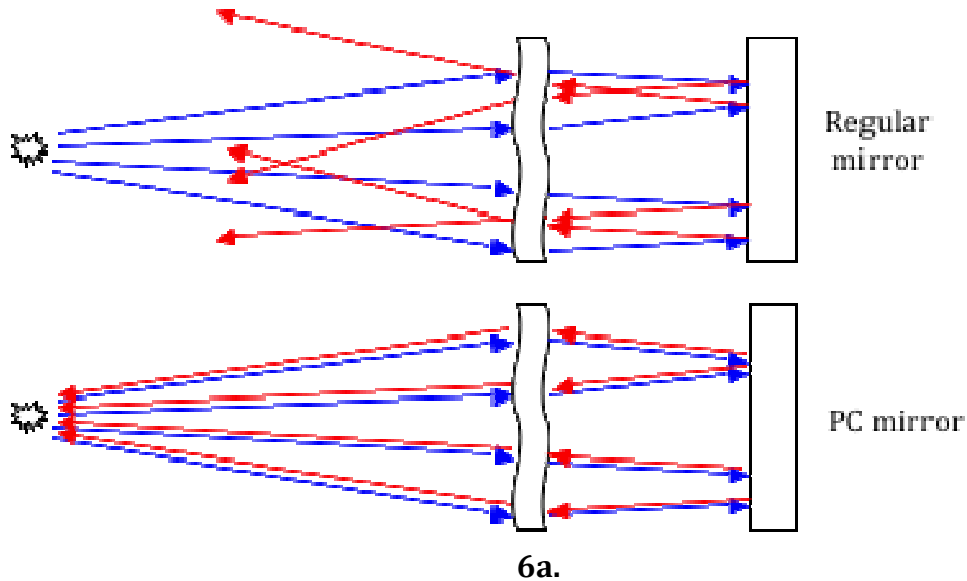
Correctly pointed, the laser appears to be shooting into empty space but, when its pulse arrives, the target is there. We literally look in two directions, separated by about 100 $\mu$ rad, sequentially. Two independent adaptive optics systems correct these paths. The acquisition path uses the target itself as guidestar. A sodium laser guidestar is tilted ahead of the detector by a computed angle, and a separate array uses the signal from that to command the corrector plate to keep the laser focus on its target during the laser pulse.

### *6.4 Rôle of Brillouin-Enhanced Four-Wave Mixing (BEFWM) in Adaptive Optics*

BEFWM (see Figure 4 and Appendix) is a type of phase conjugation in which phase distortions are automatically compensated (Kearney, et al. 2009, Kulagin et al. 1992, Zhu et al 2009, Chengyu 2008, MacDonald et al. 1988 Bespalov et al. 1986). This is important when mirror size is much larger than atmospheric turbulence cells, because conventional adaptive optics require thousands of actuators operating at a 1kHz rate.

Phase conjugation operates like holography, but it is a dynamic hologram dynamically recorded by interfering waves in a nonlinear optical medium rather than being a static pattern on a glass plate. With a phase conjugate mirror, each ray is reflected back through the system in the direction it came from with reversed

phase. This reflected wave "undoes" the distortion, converging to the initial point source. The amplified conjugate signal is automatically concentrated on the space object to an accuracy that is determined not by the turbulent scattering angle ( $\sim 100 \mu\text{rad}$ ) but, instead by the spatial resolution of the receiving aperture ( $\sim 0.1 \mu\text{rad}$  for a receiving aperture of 10 m).



LA – laser amplifier, MO – laser-master oscillator, IL – illumination laser,  $L$  – distance to target,  $D$  – primary mirror diameter,  $\theta_0$  – illumination angle

6b.

**Figure 4. How BEFWM works.** a): A phase conjugate (PC) mirror behaves differently from a regular mirror. A regular mirror reflects incident rays in the opposite direction, so that the angle of incidence is equal to the angle of reflection (see Fig.1). In contrast, light from a phase conjugate mirror is always reflected exactly in the backward direction, independent of the angle of incidence. b): A nonlinear optical cell (BEFWM) and pump laser are added to the usual laser chain to implement a BEFWM system.

A special advantage of this technique is that the target becomes its own guidestar. This is because the time by which the phase correction is “out of date” is just that required for a double pass through the atmosphere ( $\sim 100\mu\text{s}$ ), much faster than the 1ms time in which atmospheric phase distortions can typically change. A further advantage is that tilt anisoplanatism is eliminated because, during this time, the spot being corrected in the atmosphere has translated transversely by only 5mm due to slewing of the laser beam. Finally, the system has extremely narrow acceptance bandwidth, leading to good background noise rejection. Target look-ahead is computed by a proprietary technique.

It may be easier to use BEFWM than classical adaptive optics, or perhaps a hybrid system will be best.

## **7.0 Advances in Lasers**

Laser systems built and operated at Lawrence Livermore National Laboratory (LLNL) over the past decade encompass the range of energies and powers required to remove orbital debris.

One example is the solid-state heat capacity laser (SSHCL), which was built and operated in the mid-2000's. This flash lamp-pumped, solid-state laser operated in burst-mode for a period of 10 s, produced 500 J pulses and average power of  $> 10$  kW (LaFortune et al. 2004).

Since 2009 LLNL has operated the world's largest and most energetic laser, the National Ignition Facility (NIF) (Haynam et al. 2007; Moses 2009). Combined NIF's 192 laser beam produce over 3 MJ in 5-10 ns pulses at the fundamental wavelength (1053 nm), and over 1.5 MJ at the third harmonic (353 nm). Building on what has been learned and demonstrated on the NIF, LLNL is now developing designs for a laser driver for the Laser Inertial Fusion Energy (LIFE) program (Bayramian et al. 2010). This high-repetition rate (10-20 Hz), high-efficiency ( $\sim 12$ -18%) diode-pumped solid-state system will produce 8-10 kJ in a single beam at 1053 nm.

LODR requires significantly less than 1% of the NIF pulse energy, does not require harmonic conversion and does not have the laser fusion energy driver requirement to operate 24/7 with high availability. A LODR laser will be simpler, more compact and far less costly than either the NIF or the LIFE laser system (Rubenchik et al. 2010), but will leverage the experience gained and investment made over several decades of laser development, construction and operation.

## **8.0 Demonstration System**

A demonstration system could be built using a 9-m mirror and a 4.6-kJ laser to prove LODR works on targets at 400km altitude.

## **9.0 International Cooperation**

It is crucial for the LODR system to be built and operated with international protocols and agreements to avoid concerns that it is really a weapon system, and to assure safety of all space assets. This is especially true during removal of large debris objects, to closely determine the landing point, to be sure that other assets are not endangered during the descent. To do this is not technically difficult, because of the low areal number density of valuable assets at any instant (about one per 200,000 km<sup>2</sup>) compared to the ~1m<sup>2</sup> cross-section of the laser beam in space.

## **10.0 Estimated Debris Removal Cost**

We do not claim high accuracy for our cost models. An accurate model requires a thorough engineering study. However, rough system cost estimates based on the algorithms described in the Project ORION review (Phipps 1996) are useful to estimate cost per object re-entered. We estimate cost per small object removed at a few thousand dollars, and that for large objects at about \$1M each. We found that these estimates predict minimum total system cost when the cost of the laser system and the telescope are about equal. A small telescope aperture requires a disproportionately large laser pulse energy to produce the required beam intensity on a target. Similarly, a small laser pulse energy requires a disproportionately large aperture to achieve the same goal.

## **11.0 Conclusions**

We analyzed all the major aspects of laser orbital debris removal, and conclude that laser orbital debris removal will work, even for large debris objects. A LODR system should provide the lowest cost per object removed among all approaches that have been proposed. LODR is the only solution that can deal with both small and large debris. With LODR, target access is at the speed of light, redundant and agile. LODR can handle tumbling objects, while mechanical grapplers cannot. The system has multiple uses aside from general debris clearing, such as preventing collisions, increasing the accuracy of debris ephemeris and controlling where large debris impact the Earth's surface. Development and construction of the laser debris removal system offers the opportunity for international cooperation. Indeed, such cooperation will be necessary to avoid concerns that it is a weapon system and provide a framework for practical use.

## **Acknowledgment**

The authors wish to acknowledge useful discussions with Joe Carroll, Tether Applications, Inc., and with David Strafford and Brian Bradford, ITT Space Systems Division.

## References

- Allen, C. *Astrophysical Quantities*, 3<sup>rd</sup> ed., Athlete Press, London, 34, 1973
- Bayramian, A., Anklam, T., et al. Compact, efficient laser systems required for laser inertial fusion energy, Proc. Conf. Technology of Fusion Energy 2010.
- Beckers, J. Adaptive optics for astronomy – Principles, performance and applications in Annual Review of Astronomy and Astrophysics, 31, A94-12726 02-90, G. Burbidge, G. (ed.), 13-62, 1993
- Bender, M. Flexible and Low-Cost Dragon Spacecraft for Orbital Debris Removal, Proc. NASA/DARPA Orbital Debris Conference ... 2009
- Bespalov, V., Matveev, A., et al. Study of maximum sensitivity of a SBS amplifier and a four-wave hypersound phase-conjugate mirror, Izvestiya, Radiophysics series, 29, 1080–1094, 1986
- Bonnal, C. High Level Requirements for an Operational Space Debris Deorbiter, Proc. NASA/DARPA Orbital Debris Conference... 2009
- Bradley A. and Wein, L. Space Debris: Assessing risk and responsibility, Adv. Space Res. 43, 1372-1390, 2009
- Bunkin F. and Prokhorov, A. Use of a laser energy source in producing a reactive thrust, Sov. Phys. Uspekhi, 19, 561-573, 1976
- C. Haynam C. et al. National Ignition Facility Laser Performance Status, Appl. Opt. 46, 3276,2007
- Carrick, P., Mead, F., et al. Lightcraft Propulsion Technology for Low Cost Access to Space, Optics & Photonics News, 10, p. 23, 1999
- Chengyu, Z., Brillouin-Enhanced Four-Wave Mixing Phase Conjugation Mirror with Large Signals, Chinese Journal of Lasers, 35, 845-848, 2008
- Egerman, R., De Smitt, S., et al. Low-weight, low-cost, low-cycle time, replicated glass mirrors, Proc. SPIE, 7739, 77390G, 2010
- Esmiller, B. Small debris removal by laser illumination and complementary technologies, Proc. ISBEP7, AIP Conference Proceedings, to be published, 2011
- Hanada, T., Kitazawa, Y., et al. Small and Medium Orbital Debris Removal Using Special Density Material, Proc. NASA/DARPA Orbital Debris Conference... 2009
- Hansen M. and Malchow, D. Overview of SWIR detectors, cameras and applications, Proc. SPIE 6939, 693901-1 - 693901-11, 2008
- Hayhurst, C., Livingstone, I., et al. Ballistic limit evaluation of advanced shielding using numerical simulations, Int. J. Impact Engineering 26, 309-320, 2001
- Henderson, J., Nikolaev, S. et al. Intelligent sensor tasking for space collision mitigation, Proc. SPIE 7691, 76910L, 2010
- Hoyt, R. RUSTLER: Architecture and Technologies for Low-cost Remediation of the LEO Large Debris Population, Proc. NASA/DARPA Orbital Debris Conference... 2009  
<http://www.eso.org/public/teles-instr/e-elt.html>, 2011
- Kantrowitz, A. Propulsion to Orbit by Ground-Based Lasers, Aeronautics and Astronautics, 10, 74-76, 1972
- Kawamoto, S., Ohkawa, Y., et al. Strategies and Technologies for Cost Effective Removal of Large Sized Objects, Proc. NASA/DARPA Orbital Debris Conference... 2009
- Kearney, S., Valley, M., et al. Small Object Imaging and Signal Transmission through Turbulence and Debris: LDRD Final Report, Sandia National Laboratories report SAND2009-8190, 2010 (on line at: <http://prod.sandia.gov/techlib/access-control.cgi/2009/090692.pdf>)
- Kessler D. and Cour-Palais, B. Collision Frequency of Artificial Satellites: The Creation of a Debris Belt, J. Geophys. Res., 83, 2637-2646, 1978
- Klinkrad, H. Space Debris – Models and Risk Analysis, Praxis Publishing, Chichester, UK, p. 97, 2006
- Klinkrad, H. *ibid.*, p. 126
- Klinkrad, H. *ibid.*, p. 70
- Klinkrad, H. *ibid.*, p. 96

- Klinkrad, H. Space Debris Environment Remediation, Proc. NASA/DARPA Orbital Debris Conference ... 2009
- Kulagin, O., Pasmanik G., et al. Amplification and phase conjugation of weak signals, Sov. Phys. Uspekhi, 35, 506-519, 1992
- Kuznetsov, L. and Yarygin, V. Laser-reactive method for disposal of small space debris, Quant. Electron., 24, 555-557, 1994
- LaFortune, K., Hurd, R., et al. Intracavity adaptive correction of a 10 kW, solid-state, heat-capacity laser, Proc. SPIE 5333, 53-61, 2004
- Leavitt, K. NASA Ames ADR Efforts, Proc. NASA/DARPA Orbital Debris Conference... 2009
- Lee, I. An Investigation into Passive Collision Removal Methods, Proc. NASA/DARPA Orbital Debris Conference... 2009
- Liedahl, D. A., Libby, S. B., and Rubenchik, A. Momentum Transfer by Laser Ablation of Irregularly Shaped Space Debris, AIP Conf. Proc. 1278, 772-779, 2010
- Lieu, J.-C. and Johnson, N. Risks in Space from Orbiting Debris, Science 311, 340-341, 2006
- Liukonen, R. Laser rockets, Technical Physics Letters, 27, 1030-1031, 2001
- Lyon, S. and Johnson, J. SESAME: The Los Alamos National Laboratory Equation of State Database, LANL Report LA-UR-92-3407, 1992. The SESAME equation-of-state database is maintained by group T-1 at Los Alamos National Laboratory (sesame@lanl.gov).
- MacDonald, K., Tompkin, W., et al. Passive One-Way Aberration Correction Using Four-Wave Mixing, Opt. Lett. 13, 485-487, 1988
- Mason, J., Stupl, J., et al. Orbital Debris Collision Avoidance, arXiv:1103.1690v1 [physics.space-ph], 2011
- McKnight, D. Removing Orbital Debris without Going into Orbit, Proc. NASA/DARPA Orbital Debris Conference... 2009
- More, R., Warren, K., et al. D. Young and G. Zimmerman, A new quotidian equation of state (QEOS) for hot dense matter, Phys. Fluids 31, 3059, 1988.
- Moses, E. Ignition on the National Ignition Facility: a path towards inertial fusion energy, Nuc.Fus.,49, 104022, 2009
- Pearson, J., Carroll, J., et al. ElectroDynamic Debris Eliminator for Active Debris Removal, Proc. NASA/DARPA Orbital Debris Conference... 2009
- Phipps, C. An Alternate Treatment of the Vapor-Plasma Transition, Int. J. Aerospace Innovations 3, 45-50, 2011
- Phipps, C. Catcher's Mitt as an Alternative to laser Space Debris Mitigation, AIP Conf. Proc. 1278, 509-514(2010)
- Phipps, C. HICLASS Ladder Tracking Analysis final report, 1999, available from Textron Systems Corp., Wilmington MA
- Phipps, C. in Project ORION: Orbital Debris Removal Using Ground-Based Sensors and Lasers, Campbell, J. (ed.) NASA Marshall Spaceflight Center Technical Memorandum 108522, p. 221, 1996b
- Phipps, C., Birkan, M., et al. Laser Ablation Propulsion, J. Propulsion and Power, 26, 609-637, 2010
- Phipps, C., Friedman, H., et al. ORION: Clearing near-Earth space debris using a 20-kW, 530-nm, Earth-based, repetitively pulsed laser, Laser and Particle Beams, 14, 1-44, 1996a
- Phipps, C., Reilly, J., et al. Optimum Parameters for Laser Launching Objects into Low Earth Orbit, Laser and Particle Beams, 18, 661-695, 2000
- Phipps, C., Thomas S., et al. Effect of nonlinear refraction on beam brightness in laser fusion applications, Proc. Intl. Conf. on Lasers '79, STS Press, McLean VA, 878-887, 1980
- Phipps, C., Turner, T., et al. Impulse Coupling to Targets in Vacuum by KrF, HF and CO<sub>2</sub> Lasers, J. Appl. Phys., 64, 1083-1096, 1988.
- Priedhorsky W. and Bloch, J. Optical detection of rapidly moving objects in space, Appl. Opt. 44, 423-433, 2005
- Rubenchik A., et al, Laser systems for orbital debris removal, AIP Conf. Proc.1278, 347-353, 2010
- Saha, M. Ionization in the solar chromosphere, Phil. Mag. 40, 472, 1920

Simms, L., Riot, V., et al. Optical payload for the STARE pathfinder mission, Proc. SPIE 8044, 804406, 2011

Sinko J. and Phipps, C. Modeling CO<sub>2</sub> laser ablation impulse of polymers in vapor and plasma regimes, Appl. Phys. Lett. 95, 131105, 2009

Starke, J., Bischof, B., et al. ROGER, A Potential Orbital Space Debris Removal System, Proc. NASA/DARPA Orbital Debris Conference... 2009

Strafford, D. CCAT Panels: Corrugated mirror solution, [http://www.submm.org/mtg/2006/2006-01-pasadena/11\\_Borosilicate\\_Panels.pdf](http://www.submm.org/mtg/2006/2006-01-pasadena/11_Borosilicate_Panels.pdf), 2006

Strafford, D., DeSmitt, S., et al. Development of lightweight stiff stable replicated glass mirrors for the Cornell Caltech Atacama Telescope (CCAT), Proc. SPIE, 6273, 62730R, 2006

Talent, A. Prioritization Methodology for Orbital Debris Removal, Proc. NASA/DARPA International Conference on Orbital Debris Removal, Chantilly, VA, 2009

Theal, J. NASA Johnson Space Center, private communication, 1996

Wilson, B., Sonnad, V., et al. A new implementation of the INFERNO algorithm, J. Quant. Spectroscopy and Radiative Transfer, 99, 658-679, 2005

Zhu, C., et al., A composite phase conjugator based on Brillouin-enhanced four-wave mixing combining with stimulated Brillouin amplification," Laser and Particle Beams 27, 681-687, 2009

## Appendix

### A1 Introduction

This material provides additional details supporting the claims made in the main paper. We review the physics of laser momentum coupling to targets, laser orbit modification using this coupling and the constraints on the ODR beam parameters posed by propagation through the atmosphere. We also review target shape effects, acquisition and tracking, atmospheric turbulence correction, the Brillouin-enhanced four-wave mixing technique as a possible alternative to standard adaptive optics and the methods for choosing targets.

### A2 Laser Momentum Coupling

In the plasma regime, it has been shown (Phipps et al. 1988) that the relationship

$$C_m = 1.84E - 4 \frac{\Psi^{9/16} / A^{1/8}}{(I \lambda \sqrt{\tau})^{1/4}} \quad \text{N/W} \quad (\text{A1})$$

describes  $C_m$  to within a factor of two for surface absorbers in the plasma-dominated regime and pulses longer than about 100ps. Also,

$$I_{sp} = 442 \frac{A^{1/8}}{\Psi^{9/16}} (I \lambda \sqrt{\tau})^{1/4} \quad \text{s} \quad (\text{A2})$$

for the plume “specific impulse,”  $v_{plume}/g_0$ . In Eqs. (A1 and A2),

$$\Psi = \frac{A}{2[Z^2(Z+1)]^{1/3}}, \quad (\text{A3})$$

where  $A$  is the average atomic mass number. The quantity  $Z \geq 1$  is the average ionization state in the laser-produced plasma plume, and is also a function of  $(I, \lambda, \tau)$  because of its dependence on electron temperature in the plasma plume,

$$kT_e = 0.256 \frac{A^{1/8} Z^{3/4}}{(Z+1)^{5/8}} (I \lambda \sqrt{\tau})^{1/2} \quad [\text{eV}]. \quad (\text{A4})$$

The approximate value of  $Z$  is determined by applying Saha’s equation (Saha 1920),

$$\frac{n_e n_j}{n_{j-1}} = \frac{2u_j}{u_{j-1}} \left( \frac{2\pi A m_p k T_e}{h^2} \right)^{3/2} \exp(-W_{jj-1}/kT_e) \quad (\text{A5})$$

and writing

$$Z = n_e/n_i, \quad (\text{A6})$$

with

$$\sum_{j=1}^{j \max} (n_j) = n_i \quad (\text{A7})$$

Parameters in the preceding relationships are:  $W_{j, j-1}$ , the ionization energy difference between the (j-1)th and jth ionization states of the material;  $m_e$ , the electron mass; Planck's constant  $h$ ;  $c$ , the speed of light;  $I$  the incident laser intensity ( $\text{W m}^{-2}$ ); the plume electron total number density  $n_e$  ( $\text{cm}^{-3}$ );  $u_j$  the quantum-mechanical partition functions of the jth state; and  $n_j$ , the number density of each of the ionized states.

Predicting  $C_{mv}$  in the vapor regime is more complicated and two models are used, depending on the data available for a particular material. For polymers in the vapor regime for which an ablation threshold fluence  $\Phi$  ( $\text{J/m}^2$ ) has been measured, we have shown<sup>26</sup>

$$C_{mv} = \sigma / \Phi = \sqrt{\frac{2 \rho C^2 (\xi - 1) \ln \xi}{\alpha \Phi_0 \xi^2}} \quad (\text{A8})$$

$$I_{spv} = \sqrt{\frac{2 \alpha \Phi_0 (\xi - 1)}{\rho g_0^2 \ln \xi}} \quad (\text{A9})$$

For elemental materials such as aluminum for which tables of vapor pressure vs. temperature  $p(T)$  exist, e.g., the Los Alamos SESAME tables or Lawrence Livermore's QEOS or PURGATORIO-based equation of state models (Lyon 1992; More et al. 1988; Wilson et al. 2005), we can work backward from hydrodynamic variables based on wavelength-independent material parameters to the incident intensity  $I$  which must exist to balance these variables, obtaining (Phipps 2011):

$$I = \frac{pv}{a} \left( \frac{\gamma}{\gamma - 1} \right) \left[ 1 - \frac{T_0}{T} + \frac{q}{C_p T} + \frac{\gamma - 1}{2} \right] + \frac{\sigma \varepsilon}{a} T^4 + B(\tau) \quad (\text{A10})$$

$$\text{where} \quad B(\tau) = \frac{1}{a} \left[ \phi(T, x_h) + \frac{x_h \rho_s C_v (T - T_0)}{\tau} \right] \quad (\text{A11})$$

These expressions can be used to generate a numerical solution which relates ablation pressure  $p$  and vapor velocity  $v$  to  $I$  over a range corresponding to  $p(T)$  data, and we can compute the vapor regime coupling coefficient (for elemental materials such as aluminum) and specific impulse from

$$C_{mv} = p/I \quad (\text{A12})$$

$$I_{spv} = v/g_0 \quad (\text{A13})$$

In any case, we can model the transition between the vapor and plasma regimes by writing for the combined coupling coefficient,

$$C_m = p/I = [(1 - \eta_i)p_v + \eta_i p_p]/I = (1 - \eta_i) C_{mv} + \eta_i C_{mp} \quad (\text{A14})$$

where the ionization fraction (the proportion of ionized to total plume particles including the neutrals  $n_0$ )

$$\eta_i = n_i / (n_0 + n_i) \quad (\text{A15})$$

$\eta_i$  is determined numerically by iterating the process indicated in Eqs. (11-13). It is convenient to implement this iteration numerically (Allen 1973) by forming

$$S_j = \frac{n_{ij}}{n_{i,j-1}} = \frac{8.64E26}{n_e} \frac{2 u_j}{\theta^{1.5} u_{j-1}} \exp[-W_{j,j-1}/kT_e] \quad (\text{A16})$$

where  $\theta = 5040/T_e$ , and then computing the array

$$P_j = \prod_{k=1}^j S_k = \left[ \frac{n_1}{n_o}, \frac{n_2}{n_o}, \frac{n_3}{n_o}, \dots \right] \quad (\text{A17})$$

and the constants

$$R_1 = \frac{n_i}{n_o} = \sum_{j=1}^{j_{\max}} \frac{P_j}{j} \quad (\text{A18})$$

and

$$R_2 = \frac{n_e}{n_o} = \sum_{j=1}^{j_{\max}} j P_j \quad (\text{A19})$$

from which

$$Z = R_2/R_1 \quad (\text{A20})$$

and

$$\eta_i = (1 + 1/R_1)^{-1} \quad (\text{A21})$$

can be computed, as well as  $n_e = R_2 [(kT_e/p)(1+R_1+R_2)]^{-1}$  for a new iteration in Eq. (A16). (A22)

### A.3 Laser Orbit Modification

Figure A1 shows the geometrical variables for analyzing laser orbit modification. Where the zenith angle  $\phi_z = \phi - \delta$ ,  $\delta = -\sin^{-1}(r_E \sin \phi / z)$ , and  $\beta = \tan^{-1}(v_r / v_\phi)$ , range to the target is obtained from

$$z^2 = r^2 + r_E^2 - 2 r r_E \cos \phi \quad (\text{A23})$$

Using the relationships:

$\bar{i}_N \cdot \bar{i}_z = -\cos(\beta - \delta) = -\cos \xi$  and  $\bar{i}_T \cdot \bar{i}_z = -\sin(\beta - \delta) = \sin \xi$ , and with the Hamiltonian  $(E + V)$ , expressed in unit mass variables,

$$E = \frac{(v_r^2 + v_\theta^2)}{2} \quad \text{and} \quad (\text{A24})$$

$$V = -GM/r, \quad (\text{A25})$$

the eccentricity

$$e = \frac{r_a - r_p}{r_a + r_p}, \quad (\text{A26})$$

where  $r_a$  and  $r_p$  are the apogee and perigee orbit radii. In the plane of motion, the orbit is

described by 
$$r(\phi) = \left[ \frac{r_p(1+e)}{1+e \cos(\phi + \phi_o)} \right] \quad (\text{A27})$$

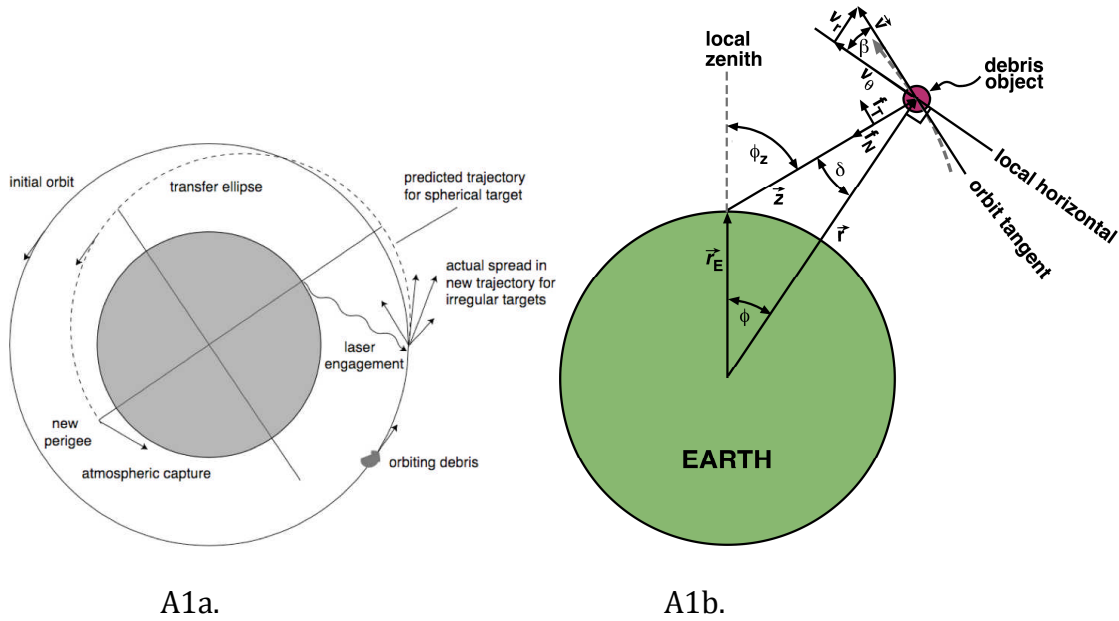


**Figure A1. Geometry of the laser-target interaction (scales exaggerated for clarity).**

**a:** Schematic of debris de-orbiting concept in low-Earth orbit. For a given energy deposition, the orbital perturbation on a spherical target is predictable. For non-spherical targets, the perturbation can be predicted, if the shape and orientation at engagement are known.

**b:** Thrust on a debris object is resolved into components  $f_T$  and  $f_N$  normal to and along the orbit tangent. Since, for LEO debris, range  $z \ll$  the Earth's radius  $r_E$ , the zenith angle  $\phi_z$  changes rapidly compared to the geocentric angle  $\phi$ .

a definition which means perigee is at  $\phi = \phi_0$ . Where  $r_p$  is the perigee geocentric radius, and the semi-major axis  $a = r_p / (1 - e)$ ,  $l$  is the angular momentum per unit mass,  $MG$  is the Earth's gravitational constant and the quantity

$$q = a(1 - e^2) = l^2 / MG, \quad (\text{A28})$$

the tangential and radial velocity components are

$$v_\phi = \sqrt{\frac{MG}{q}} [1 + e \cos(\phi + \phi_0)] \quad \text{and} \quad (\text{A29})$$

$$v_r = \sqrt{\frac{MG}{q}} [e \sin(\phi + \phi_0)]. \quad (\text{A30})$$

The total velocity is obtained from  $v^2 = v_r^2 + v_\phi^2 = MG \left( \frac{2}{r} - \frac{1}{a} \right)$ . (A31)

For externally perturbed orbits, we have

$$\Delta a = \frac{GM}{2H^2} \Delta H, \quad (\text{A32})$$

and 
$$\Delta v_r = -\Delta J_N = +\Delta J \cos \xi \quad (\text{A33})$$

$$\Delta v_\theta = +\Delta J_T = +\Delta J \sin \xi \quad (\text{A34})$$

where  $\xi = \beta - \delta$ . Also, 
$$\Delta q = 2r\sqrt{p/MG}[\Delta J_T \cos \beta + \Delta J_N \sin \beta], \quad (\text{A35})$$

or, in a more useful form, 
$$\Delta q = \frac{2r}{v}[\Delta J_T(1 + e \cos(\phi + \phi_o)) + \Delta J_N e \sin(\phi + \phi_o)] \quad (\text{A36})$$

In Eq. (A36),  $\Delta J_T$  and  $\Delta J_N$  are, respectively, the components of  $\Delta \vec{J}$  along the orbit tangent, and along the inward normal to the orbit in the orbital plane. This equation makes the point that  $\Delta J_N$  also has a major effect on the orbit, not  $\Delta J_T$  alone as one might intuitively think. The magnitude of  $\Delta J$  is related to laser and target variables by

$$\Delta J = \eta_c C_m \Phi / \mu \quad (\text{A37})$$

using terms defined in Eq. (6) of the main paper.

When  $(\phi + \phi_o) = 0$  [perigee at zenith], Eq. (A36) shows  $\Delta J_N$  has no effect. Since  $\Delta H = v_r \Delta v_r + v_\theta \Delta v_\theta$  and  $v_r = 0$  at perigee, even a large  $\Delta v_r$  can have no significant effect. The effect of pushing directly upward is to instantaneously tilt the velocity vector upward, so that the orbit can change later. In the majority of cases, the perigee or apogee will not be directly overhead, and calculations show we can drop perigee by pushing directly upward on the object.

Now, 
$$\Delta H = v_r \Delta v_r + v_\theta \Delta v_\theta, \quad (\text{A38})$$

$$\Delta v'^2 = v'^2 - v^2 = 2\Delta H, \quad (\text{A39})$$

But, since 
$$\Delta q = (1 - e^2)\Delta a - 2ae\Delta e, \text{ we can write} \quad (\text{A40})$$

giving 
$$\Delta e = \frac{[(1 - e^2)\Delta a - \Delta q]}{2ae} \quad (\text{A41})$$

From which, 
$$\Delta r_p = (1 - e)\Delta a - a\Delta e \quad (\text{A42})$$

□ □ □ 
$$\Delta r_a = (1 + e)\Delta a + a\Delta e \quad (\text{A43})$$

If  $e = 0$ , Eq. (A40) gives correct results in the limit  $e \rightarrow 0$ .

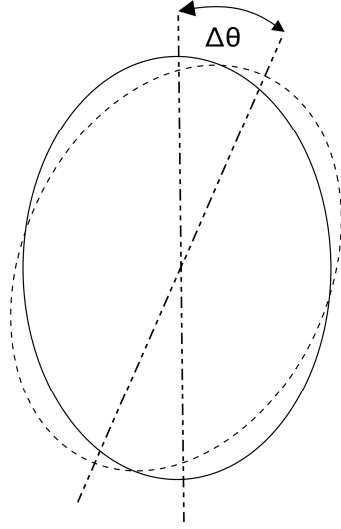


**Figure A2.** Apsidal shift

To apply these relationships, we substitute  $\Delta J$  from Eq. (A37) into Eqs. (A33) and (A34) to obtain the radial and azimuthal components of the laser-induced target velocity change, and the parameter  $\Delta q$  using Eq. (A36). Then, we substitute the velocity increments into Eq. (A38) to get  $\Delta H$ , and use this to get  $\Delta a$  in Eq. (A32). Now we can compute  $\Delta e$  from Eq. (A41) and, using that,  $\Delta r_p$  and  $\Delta r_a$  from Eqs. (A42) and (A43). This procedure is developed from first principles rather than involving intermediate relationships and is free of approximations.

Next, we have the problem of calculating the rotation angle of the semi-major axis of the ellipse due to our actions [Figure A2]. If it's too large, might unintentionally raise something we earlier lowered. Axis rotation can be computed. We use  $\Delta\beta$  after the interaction, and  $d\beta/d\phi$  for the original ellipse, to find

$\Delta\theta$ .

$$\text{Since } \frac{d\beta}{d\phi} = \frac{d\beta}{dr} \frac{dr}{d\phi} \quad (\text{A44})$$

$$\text{and } \frac{dr}{d\phi} = -(er^2/p)\sin(\phi+\phi_0), \quad \text{with } m = (2r-r^2/a)$$

$$\text{and } p=a(1-e^2), \quad \frac{d\beta}{d\phi} = \frac{-(1-r/a)er^2}{[1-p/m]^{1/2} m^{3/2} \sqrt{p}} \sin(\phi+\phi_0) \quad (\text{A45})$$

$$\text{and } \Delta\theta = -\frac{\Delta\beta}{d\beta/d\phi} \quad (\text{A46})$$

is easily calculated. For small debris, which can be re-entered in a single pass, this apsidal shift is irrelevant. For large debris, it must be taken into account when the object is re-engaged. The preceding analysis is most useful for calculating total perigee reduction as in Figure 3 of the main text.

### A3.1 Optical Constraints from the Atmosphere and Target Physics

In a Laser ODR system design, we must simultaneously satisfy the constraints that arise from diffraction, nonlinear optical effects in the atmosphere and target physics. Beam fluence in the atmosphere is constrained above and below. Where  $z$  is target range,  $\lambda$  is wavelength,  $D_{\text{eff}}$  is launching aperture diameter, we use the symbol

$$\zeta = \frac{az\sqrt{\lambda}}{D_{eff}^2} \quad (A47)$$

to represent the effects of diffraction, and find that a lower limit for beam fluence in the atmosphere is given by

$$\frac{\Phi_b}{\lambda} \geq \frac{\beta\zeta^2\sqrt{\tau}}{T}, \quad (A48)$$

in order to ignite a plasma on the target. We assume a beam quality factor of 2 and an index 6 hypergaussian radial intensity profile, which together give  $a = 1.7$  in Eq. (52), so a typical value of  $\zeta$  is 75. In Eq. (A48),  $T$  is atmospheric transmission, which we take to be 85%.

The upper limit beam fluence is set by nonlinear optical (NLO) effects including (for short pulses) phase distortions due to nonlinear index ( $n_2$ ) and stimulated rotational Raman scattering (SRS) and stimulated thermal Rayleigh scattering (STRS). For pulses  $100\text{ns} \leq \tau \leq 1\text{ms}$ , the NLO effects limit amounts to  $\Phi_b/\lambda \leq 3E10 \tau \text{ Jm}^{-2}\mu\text{m}^{-1}$ . For shorter pulses, this linear dependence saturates, settling at  $\Phi_b/\lambda \leq 100 \text{ J m}^{-2}\mu\text{m}^{-1}$  at 100ps. We can obtain solutions to these twin requirements graphically.

### A3.2 Target Shape Effects

To draw attention to the variety of debris shapes and materials, the ORION project study [Phipps 1996b] described five representative compositional classes:

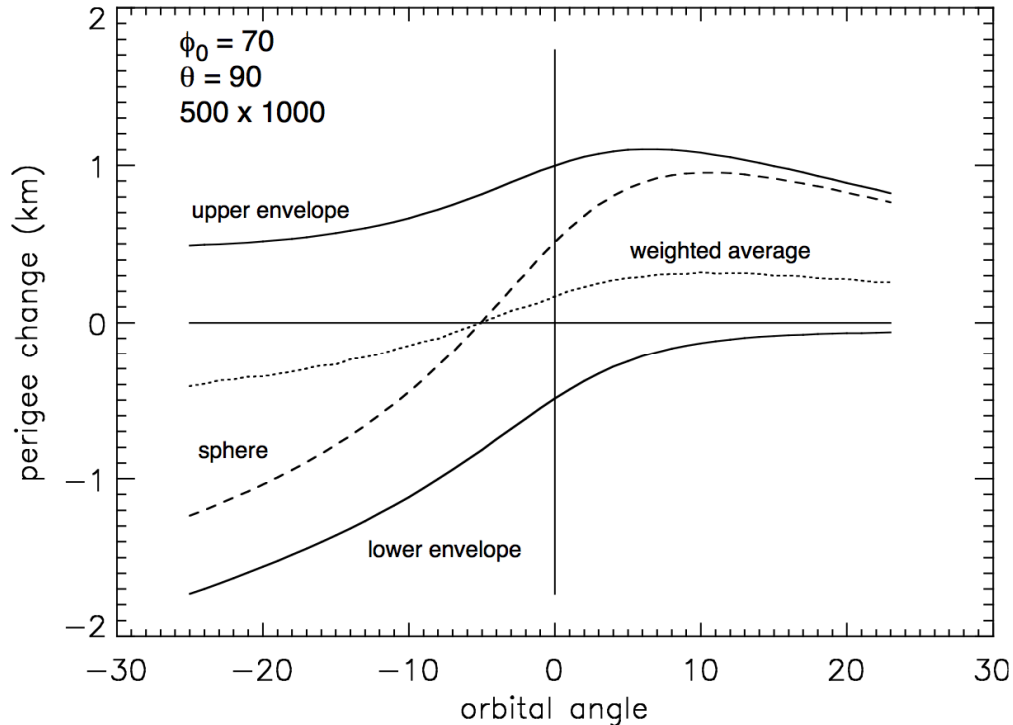


**Figure A3. Calculated perigee change.** A 1 gram plate receives a single 10 J pulse on the debris target at the indicated geocentric angle, with  $C_m = 100 \mu\text{N}\cdot\text{s}/\text{J}$ , assuming a random distribution of plate orientations in three dimensions, perigee change plotted against orbital angle. Negative angles correspond to upstream positions relative to the laser position at  $\phi=0$ . Horizontal extent of abscissa maps to laser horizons. Example orbit is characterized by 500 km perigee, 1000 km apogee, perigee angle ( $\phi_0$ ) 70 degrees downstream of the laser position (descending), with an orbit intersecting laser zenith. Plotted are the best case (“lower envelope”), worst case (“upper envelope”), the weighted average (dotted), and the single-valued result for a spherical target (dashed).

aluminum, steel, sodium-potassium spheres, carbon phenolic, and metal-coated plastic insulation. Only a fraction of these have spherical symmetry. The existence of irregularly shaped space debris brings a degree of randomness into the problem of calculating post-engagement orbital modifications: that associated with the distribution of object shapes, and that associated with orientation. Given the desire to reduce perigee, it is of interest to characterize the range of possible orbital outcomes of laser engagements with non-spherical targets (Figure A3)(Liedahl, et al. 2010).

In general, the impulse and laser propagation vectors are not parallel. Since ablation will be parallel to the local normal, and the impulse is directed opposite to the net ablation vector, we can write

$$m\Delta\bar{v} = -C_m\Phi_L \sum_{\alpha} A_{\alpha} \left| \hat{k} \cdot \hat{n}_{\alpha} \right| \hat{n}_{\alpha} \quad (\text{A49})$$

summing over all illuminated surface elements  $A_{\alpha}$ , and the laser fluence is given by  $\bar{\Phi}_L = \Phi_L \hat{k}$ . For “smooth” objects, the sum goes over to an integral over the illuminated portion of the surface. For illustration, we choose the simple case of a plate of mass  $m$ , in a low elliptical orbit, with eccentricity given by

$$\varepsilon = \left( 1 + \frac{2EL^2}{G^2M^2m^3} \right)^{1/2} \quad (\text{A50})$$

where  $E$  is the total orbital energy,  $L^2$  is the square of the orbital angular momentum,  $G$  is the gravitational constant, and  $M$  is Earth’s mass. After engagement, a new orbit is determined from changes to  $E$  and  $L^2$ . If the instantaneous distance from Earth’s center, orbital velocity, and azimuthal velocity are denoted  $r$ ,  $v$ , and  $v_{\phi}$ , respectively, then  $\Delta E$  and  $\Delta L^2$  are given in terms of the velocity change by

$$\Delta E = m\bar{v} \cdot \Delta\bar{v} + \frac{1}{2} m |\Delta\bar{v}|^2 \quad (\text{A51})$$

$$\Delta L^2 = 2m^2r^2v_{\phi} \Delta\bar{v} \cdot \hat{\phi} + m^2r^2 (\Delta\bar{v} \cdot \hat{\phi})^2 \quad (\text{A52})$$

The quantity of primary interest is the perigee, which is

$$r_p = \frac{l^2}{GMm^2} \frac{1}{1+\varepsilon} \quad (\text{A53})$$

We calculate the perigee change for a random distribution of plate orientations, and for a representative set of orbital parameters, setting  $m = 1$  g for this example. The maximum laser energy on target is 10 J, which occurs when the plate is face-on to the laser position. The distribution in the perigee change at a fixed orbital angle (not shown) is weakly peaked, with substantial probability at the upper and lower bounds. Thus one can estimate the probability of achieving an undesirable result, i.e., an increased perigee, by comparing the magnitude of the upper and lower envelopes. It is also worth noting that there is a non-negligible probability of achieving a result that is *more* favorable than for the spherical case. The average perigee change for a plate is approximately 1/3 that found for a sphere, which has implications for the efficiency of targeting campaigns. Of course, this efficiency can be increased substantially by intelligently timing the laser pulse when the target and its surface orientation can be resolved.

It is possible for an irregularly shaped target to ablate in such a way as to create a torque about the center of mass, resulting in spin. The change in spin

energy can be comparable to the change in kinetic energy. Additionally, it is known that some space debris fragments are already spinning, which means that interactions with a laser may alter the spin frequency, and may alter the orientation of the spin vector. When spin in an asymmetric debris fragment is present (or is induced), the laser/target interaction will vary from shot to shot, resulting each time in a different impulse, which leaves a complex scenario for targeting and re-acquisition. However, spin is beneficial; with several hundred engagements, the range of possible orientations becomes well sampled, and the overall effect will tend toward the mean, producing results like those in Figure A3.

#### **A4 Acquisition and Tracking**

Note that an array of guidestars may be needed to correct for focal anisoplanatism well enough to achieve the highest possible brightness on target. Rayleigh beacons, which just use scattering from the atmosphere rather than exciting the sodium layer may also be used. These are in some ways less effective, because the effective point source is closer, but have the advantage of being at the same wavelength as the pusher laser.

##### *A4.1 An Alternative Target Tracking Method*

For active tracking, an alternate method has already been proven at the U.S. Air Force Maui Space Surveillance System (MSSS) in Hawaii. Located on the crest of Mt. Haleakala at an elevation of 3060 meters, it is also a good site for LODR because of better seeing conditions than possible at sea-level sites. One component is the Advanced Electro-Optical System 3.67-m diameter telescope at MSSS, with recoated dichroic optics and a modified coudé path. The other is the 11.2 $\mu$ m wavelength "HICLASS" 900W pulsed CO<sub>2</sub> laser and its heterodyne detection system, which, together, have been shown (Phipps 1999) to be able to easily track sub-cm objects at 1000km range. This performance comes about because the system is located at a cold, high altitude site, because it achieves near photon-counting performance, and because there are nine times as many photons per joule at its wavelength, compared to 1.06 $\mu$ m. Using this system, it should be possible to acquire and track 100 times as many targets per hour at 1000km range, these targets being twice as small, as with radar (Klinkrad 2006, *ibid.* p. 126).

##### *A.4.2 Turbulence Correction with Standard Adaptive Optics*

Figure A4 shows a possible telescope design to implement the LODR system discussed in the main paper, incorporating conventional adaptive optics. At the bottom of the figure A4, a deformable mirror with many computer-controlled piezoelectric actuators creates a deformation in the high power laser input phase front which exactly cancels phase distortions in the atmosphere, moment by moment. Typically, a control system bandwidth of about 1kHz is required to do this. Atmospheric phase distortions are sensed by AO unit no. 1, which is pointed at the sodium guidestar which has been set up at 90km altitude by a 589.2 beacon beampath projected by the telescope (not shown). This works by exciting sodium

atoms already present at that altitude, to create what is nearly a point source viewed from the ground. Knowing this, the AO system works until it sees a point source; the resulting phase shape is recorded and reversed at the deformable mirror. Of course, the laser and the guidestar are at two different wavelengths, so the computer has to attempt to calculate what the distortion should be at  $1.06\mu\text{m}$  from what it knows at  $589.2\text{nm}$ , and this is not always accurate.

The Figure shows a suggested layout for the telescope discussed in the main paper, in which standard adaptive optics are used to correct atmospheric turbulence. Two other AO systems (no. 2 and no. 3) in the figure correct phase distortions at  $1.06\text{mm}$  directly, using the target itself as a point source guidestar, in order to acquire the target with optimum resolution.

Why then do we need the sodium guidestar? This is because AO systems no. 2 and no. 3 are pointing in a different direction from the high power laser, at the object where it appears to be. In contrast, the high power laser, in contrast, has to fire into black space along a different path with different distortions at the spot where the target is predicted to be when its beam arrives. So, we need an artificial guidestar to facilitate phase correction along the high power beam path.

#### *A4.3 Turbulence Correction by Brillouin-Enhanced Four-Wave Mixing*

An alternative to standard adaptive optics for correcting phase distortions along the path occupied by the high power laser beam is called Brillouin-enhanced Four-wave Mixing (BEFWM). As in the standard AO technique, we depend on a few photons scattered back into the telescope when we fire the high power laser beam at the target. The debris object's reflected illumination is intercepted by the main mirror of a receiving telescope and guided to optical brightness amplifiers. After amplification, the object's image is recorded with a CCD camera.

A control system turns on the brightness amplifiers and adjusts their reception frequency band. Data for the control system are provided by an illumination laser and a rangefinder that estimates moment of arrival of the scattered radiation and its frequency. The optical brightness amplifiers consist of three units: a laser amplifier, a nonlinear optical amplifier and a pump laser. To achieve the lowest level of noise in the optical brightness amplifiers, the laser amplifier gain coefficients must be about  $1\text{E}4$ . Such a gain coefficient can be achieved in two amplification stages. When creating the laser amplifiers, it is

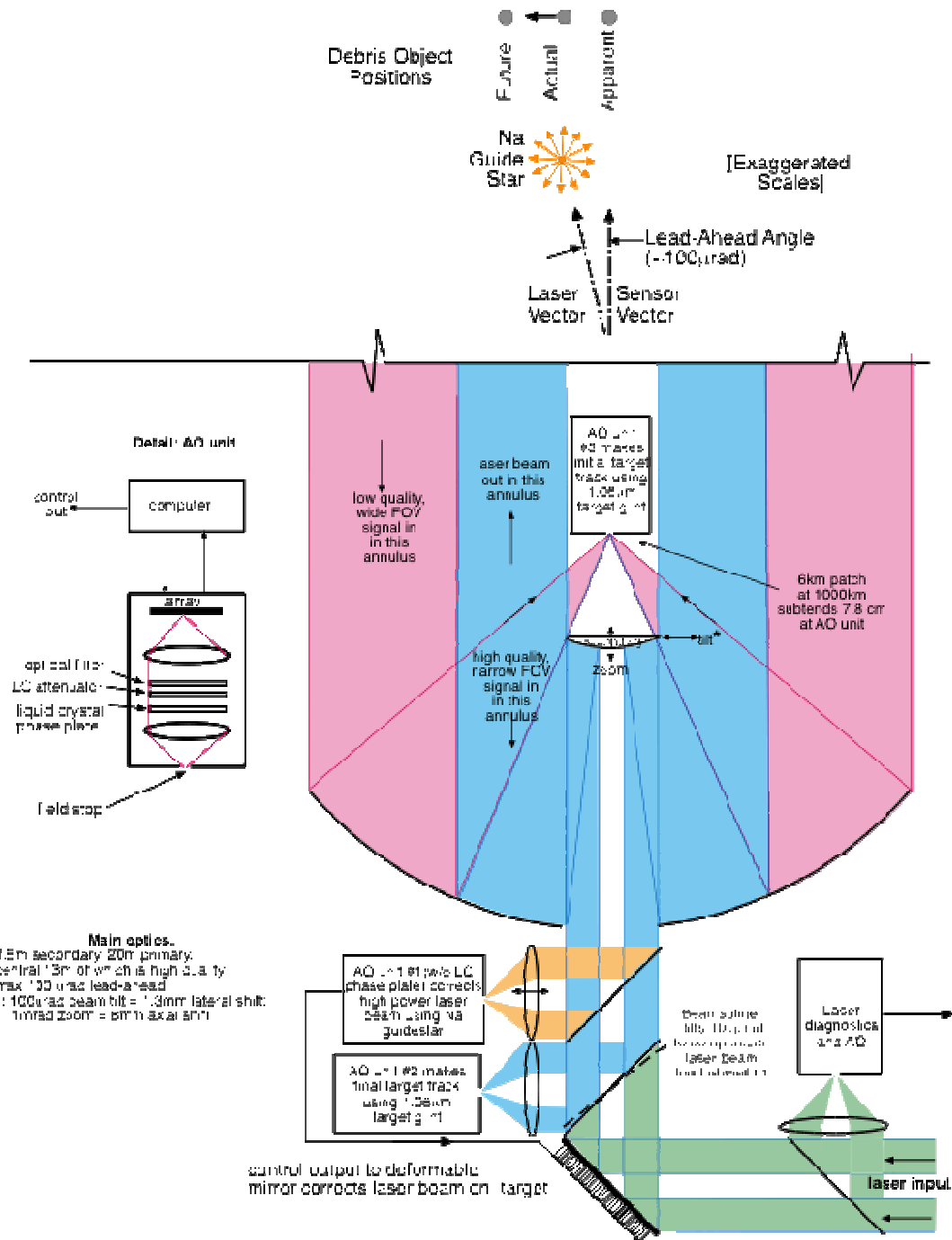


**Figure A4.** A possible telescope design discussed in the main paper, including conventional adaptive optics.

necessary to ensure that the value of the gain coefficient is uniform over the whole field of vision. The latter, in turn, should be not less than the angle of initial illumination  $\Delta\phi = 1\text{E-}4$  radians, which requires the use of optical repeaters. The space object plane is projected by a lens onto the output face of the first laser amplifier. The image is then transferred by a repeater from the output face of the first laser amplifier to the input of the second laser amplifier. Another repeater transfers images from the output face of the second laser amplifier to the nonlinear optical amplifier. The repeater is a confocal telescope.

The nonlinear optical amplifier is a Stimulated Brillouin Scattering (SBS) amplifier (a third order nonlinear medium which is active with respect to the Brillouin nonlinearity). For such a medium to amplify signal light, it should be illuminated simultaneously with the space object reflected signal and by a powerful additional laser radiation pump. Typical nonlinear medium elements are tetrachlorides such as  $\text{CCl}_4$ ,  $\text{GeCl}_4$ ,  $\text{SnCl}_4$ , or perfluorooctane. Their parameters are very similar (nonlinearity factor  $\sim 5\text{E-}9$  cm/W, and hypersound relaxation time  $\sim 1\text{ns}$ ). When the SBS cell is illuminated by a pulsed laser with energy 1.5 J and duration 20 ns, the SBS amplifier amplifies the space object scattered light with a gain coefficient of approximately  $1\text{E}8$ . Therefore, the gain coefficient of light received from the space object, consisting of combined gain in laser amplifier and nonlinear optical amplifier, will be about  $1\text{E}12$ , which is adequate to create a recordable image.

The concentration of the space object reflected laser illumination is restricted by the influence of turbulence. To improve imaging and to minimize the required level of illumination laser irradiance to make a jet on the target requires that we overcome the atmospheric turbulence to focus the beam. This is achieved through optical phase conjugation of the illumination radiation using BEFWM to reverse the beam propagation direction and phase to compensate for atmospheric distortions as the beam back propagates through the optically distorting path. If our nonlinear-optical receiver amplifies and conjugates the signal intercepted by the receiving lens, then as a result of double passage through the atmosphere turbulent distortions of the space object signal wavefront are compensated. Consequently, the conjugated signal will be concentrated on the space object to an accuracy that is determined not by the turbulent scattering angle ( $\sim 10$   $\mu\text{rad}$ ) but, instead by the resolution of the receiving aperture of the nonlinear optical amplifier (e.g.,  $\sim 0.05$   $\mu\text{rad}$  for a receiving aperture of 20m).

#### *A4.3.1 How BEFWM Works*

A number of papers are available concerning laser propulsion (Kantrowitz 1972; Carrick et al 1999; Bunkin and Prokhorov 1976; Kuznetsov and Yarygin 1994; Liukonen 2001). System risks are low. This kind of operation on debris will not generate additional debris. Laser irradiation of large operating spacecraft will not seriously affect them, unless photo-sensitive equipment is exposed, since under the worst conditions only very small amounts of surface material are ablated.

Phase Conjugation (PC) is a non-linear optical effect that forms the same wavefront as an initial one, but which propagates exactly in the backward direction

with reversed phase. A phase conjugate mirror is like a mirror reflecting incident light back towards where it came from, but it does so in a different way than a regular mirror. A regular mirror reflects incident rays in the opposite direction, so that the angle of incidence is equal to the angle of reflection (see Fig 4a of the main paper). In contrast, light from a phase conjugate mirror is always reflected exactly in the backward direction, independent of the angle of incidence.

This difference provides significant opportunities. If we place a distorting medium (e.g., a turbulent air flow) in the path of a beam of light, the rays radiated from the point-like light source are bent in random directions, and after reflection from a normal mirror, each ray of light is bent even farther causing the beam to scatter. With a phase conjugate mirror, on the other hand, each ray is reflected back in the direction it came from. This reflected conjugate wave propagates backwards through the same distorting medium, and "undoes" the distortion, causing the beam to converge to its initial point source.

Phase conjugation operates somewhat like holography, but it is a dynamic hologram whose "holographic plate" is determined by interfering waves in a nonlinear optical medium rather than etched as a static pattern on a glass plate. In our case, the physical mechanism of this process is called four-wave mixing because it is based on the interaction of laser waves and hypersonic waves. Here the interference of signal and pump laser waves creates a hypersonic grating and the second pump scattering on this grating produces a conjugated wave (Fig. A5). This interaction of laser waves with hypersound is known as stimulated Brillouin scattering and this type of four-wave mixing is called Brillouin enhanced four wave mixing (BEFWM). Figure A6 shows how a laboratory BEFWM setup works (Kulagin et al 1992).

This combination of laser amplifiers and the BEFWM PC mirror provides a unique set of capabilities that can enable and simplify the design of our debris removal system:

- The system has very high sensitivity near  $4.8E-19$  J per pixel (approximately two photons) which lets us minimize the laser pulse energy needed to generate a measurable scattered signal from the orbital debris.
- The system's extremely narrow frequency band corresponds to two frequency-temporal modes (input spectral bandwidth  $\sim 1$  pm and response time of  $\sim 30$  ns) which ensure our proposed system will reject background noise and engage extremely quickly to enable its use on hypervelocity debris.
- The system has a comparatively wide field of view that can be tailored to operational needs as part of the system design.
- The system has a high coefficient of amplification, amplifying weak signals by a factor of about  $1E12$ .

With the concept illustrated in Figure A6, we begin by illuminating the detected orbital debris with an initial laser pulse. An input lens receives the scattered illumination from the debris to form an object image, but as this signal pulse (carrying the image) propagates through the system it is also amplified by a preliminary laser amplifier. In turn, a PC-mirror input lens focuses the object image in the PC-BEFWM mirror. This PC-mirror is a liquid cell filled with a nonlinear

optical medium (typically, high-purity liquid tetrachlorides or freons) that is pumped by two pump pulses. The reflected conjugated pulse goes back to the object plane and on its way is partially reflected by the beam-splitter to the recording system (a CCD or CMOS camera), where an image of the space object is formed to allow us to identify the object as debris or not.

#### *A.5.3.2 BEFWM system concept of operations*

The system shown as Figure 4b of the main paper uses a BEFWM receiver-amplifier. First, a master oscillator MO delivers an illumination pulse of about 30ns duration at  $1.06\mu\text{m}$  that is amplified by the illumination laser IL and directed to the region of space containing the debris target in a comparatively wide angle of about  $100\mu\text{rad}$ . Then, part of the reflected illumination is received by an input/output (IO) mirror with clear aperture  $D$ , amplified and reflected by our BEFWM system and directed back toward the debris by the IO mirror. Phase conjugation provided by the 5 effects of atmospheric turbulence and provides perfect illumination on the debris with this second pulse, resulting in a higher quality image. The second pulse reflection from the debris may, in turn, be used to repeat this cycle to increase the lighting level, or to concentrate the laser on the debris providing a high quality glint that can be used as a target designator or to enable advanced adaptive optics methods with a guidestar maintained on the moving debris.

We assessed the concentration efficiency of the proposed system to assess the appropriate illumination pulse energy with secondary illumination using BEFWM and without it. For debris sizes on the order of 10 cm that are within a 1000 km range, we found that to image this debris without PC-adaptive optics requires high pulse energy (up to 100 kJ) for the initial illumination.

However, a one-step or two-step laser energy concentration using our system provides debris imaging with reduced initial illumination pulse energy of  $\sim 1\text{kJ}$  or even 100 J.

It should be mentioned here that a primary mirror maybe of poor optical quality (reducing initial costs) because phase conjugation will correct for its distortions too. This concept should satisfy the basic requirements in terms of laser pulse delays, laser frequencies, and precise control of the pointing and signal tuning to compensate for the debris motion and Doppler shift.

Some years ago we developed a two-pulse master oscillator (MO) with controlled delay between the two pulses to compensate for the path difference between the signal and pump pulses on the way to the BEFWM-mirror, since both of the pulses must arrive there simultaneously and their frequencies should be the same.

#### *A.4.3.3 Long-distance open-air BEFWM demonstration*

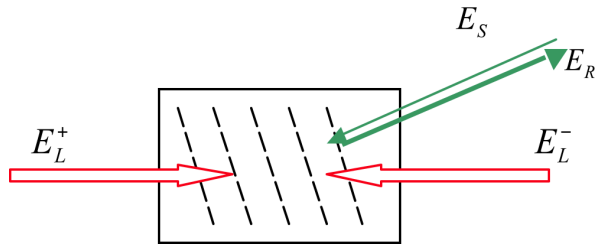


**Figure A5.** Illustrating the BEFWM process

This heating increased the structural parameter of atmospheric turbulence by a factor of 5-10, corresponding to a propagation path of several km. Our test path with air heaters and target area at the background is shown in Fig. A7 (left image). Laser energy concentration was demonstrated in the experiments. The target area is shown in the right image. We used a glass spherical reflector on a tripod to imitate a point target.

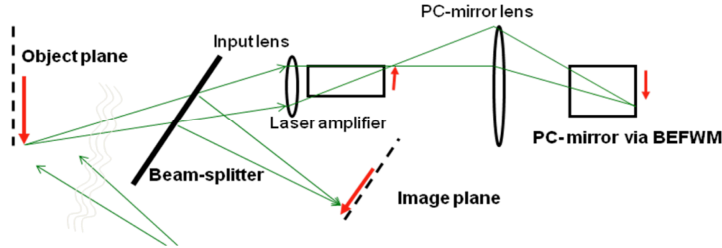


**Figure A6.** BEFWM in the laboratory

reflected and concentrated by BEFWM) simultaneously. Using an oscilloscope placed in the target area we verified that the second pulse with less total energy has a much higher laser energy density. To demonstrate this fact, a glass beam-splitter was placed in front of the spherical reflector to reflect part of the signal to a fast photo-diode. We achieved similar results in other experiments carried out on a 2.1km path and with pulse energy up to 100 J. We concluded that we can mitigate atmospheric turbulence to provide near diffraction limited images and focus a pulsed laser on orbital debris.

## A.6 Choosing Targets

The LODR system target selection balances priority with routine tasking operations, which include laser and surveillance system tasking for efficient utilization of resources. Based on SOCRATES and other space surveillance and conjunction estimates already supported by the USAF, priority operations will task the LODR to deflect a potential threat to a high value asset such as Space Station by applying a  $\Delta v$  as small as 20 m/sec, and tasking additional surveillance for post illumination track maintenance.

Routine space debris clearing will select targets with acceptable engage ability and safety. The overall concept of operations is expected to consider

We assembled and tested our non-linear optical image amplifier scheme in outdoor experiments through turbulence (Kearney et al 2010). Our path length for open air experiments was short (150m), so we developed a method of controlled turbulence intensification using banks of heaters to simulate a longer path.

In the upper right corner of Figure A7 there is a print of initial illumination of a point-like target.

The second picture is a print of both pulses (the initial pulse and the pulse

uncertainties in target cross section, orientation and spin rate, target materials and

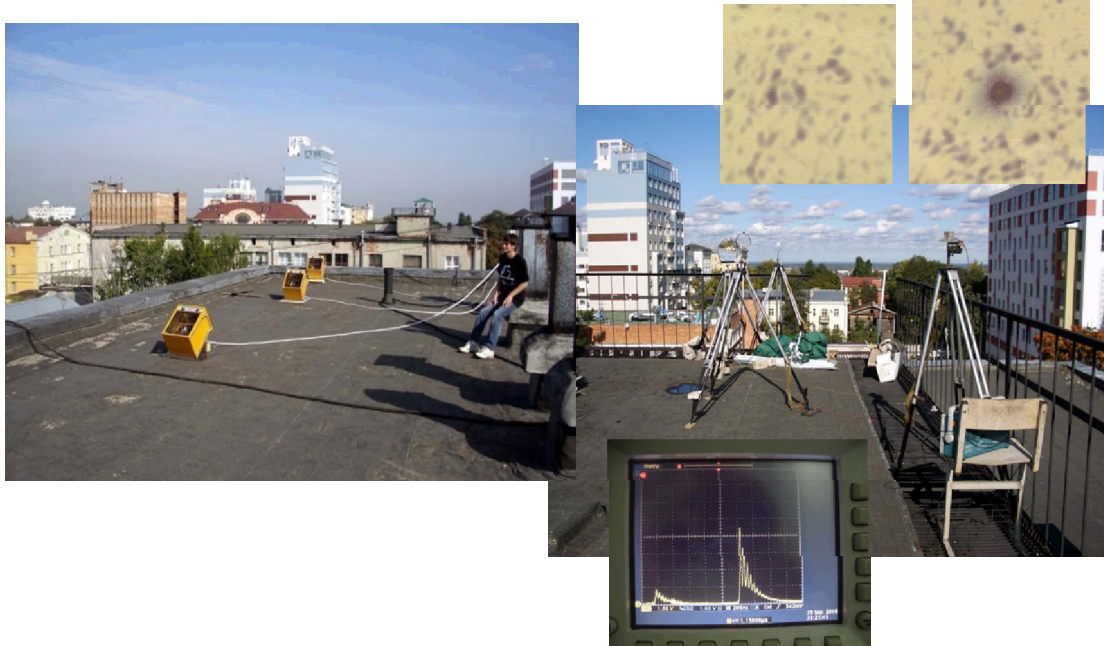


**Figure A7.** Highlights of open-air BEFWM experiments

mass, required  $\Delta V$  for assured re-entry and potential for fragmentation and collateral threat. Smaller debris single pass target illuminations at low laser beam elevations will be most effective by slowing the target by 50 to 200 m/sec and thus dropping its perigee for a rapid re-entry. Larger and heavier targets will require a multi-orbit plan for gradually lowering the perigee, and additional surveillance

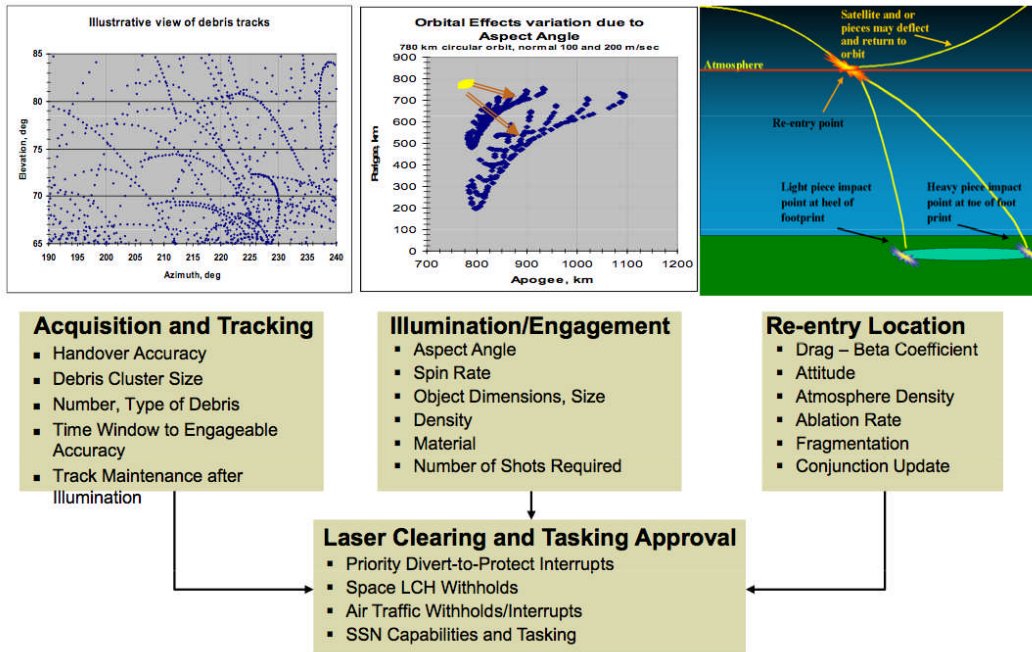


**Figure A8.** Balancing four areas of uncertainty

resources will be needed to maintain tracking on a perturbed orbit with potentially changed drag characteristics. A dual site LODR would provide additional access and response capability. Figure A8 outlines the concept of operations.

Prepared by LLNL under Contract DE-AC52-07NA27344.